Some New Results on Electron Transport in the Atmosphere*

MARTIN J. BERGER and STEPHEN M. SELTZER
National Bureau of Standards, Washington, D.C. 20234, U.S.A.

and

KAICHI MAEDA
NASA-Goddard Space Flight Center, Greenbelt, Md. 20771, U.S.A.

Abstract. The penetration, diffusion and slowing down of electrons in a semi-infinite air medium has been studied by the Monte Carlo method. The results are applicable to the atmosphere at altitudes up to ~ 300 km. Most of the results pertain to monoenergetic electron beams injected into the atmosphere at a height of 300 km, either vertically downwards or with a pitch-angle distribution isotropic over the downward hemisphere. Some results were also obtained for various initial pitch angles between 0° and 90°. Information has been generated concerning the following topics: (a) the backscattering of electrons from the atmosphere, expressed in terms of backscattering coefficients, angular distributions and energy spectra of reflected electrons, for incident energies T_0 between 2 keV and 2 MeV; (b) energy deposition by electrons as a function of the altitude, down to ~ 80 km, for T_0 between 2 keV and 2 MeV; (c) the corresponding energy deposition by electron-produced bremsstrahlung, down to ~ 30 km; (d) the evolution of the electron flux spectrum as function of the atmospheric depth, for T_0 between 2 keV and 20 keV. As far as possible, the results have been expressed in a scaled form which reduces the explicit dependence on, and permits interpolation with respect to, T_0. Energy deposition results are given for incident electron beams with exponential and power-exponential spectra.

---

1. INTRODUCTION

In the course of earlier Monte Carlo calculations of auroral luminosity patterns (BERGER, SELTZER and MAEDA, 1970; to be referred to as BSM) and bremsstrahlung flux spectra in the atmosphere (BERGER and SELTZER, 1972) we have obtained other electron and bremsstrahlung transport results which may be useful for the analysis and interpretation of observed atmospheric phenomena. These results are given here, and pertain to the following topics: (a) the backscattering of electrons from the atmosphere, as the result of multiple Coulomb scattering; (b) the altitude-dependence of energy deposition by electrons precipitated into the atmosphere; (c) the corresponding altitude-dependence of energy deposition by electron-produced bremsstrahlung; and (d) the modification of the energy spectrum of electron beams as they penetrate down into the atmosphere.

2. MONTE CARLO MODELS

The Monte Carlo method involves the simulation of all important physical processes by random sampling. One must sample the elastic scattering of electrons by atoms, the inelastic scattering of electrons by orbital electrons, the production of bremsstrahlung, and the Compton scattering and photoelectric absorption of the bremsstrahlung photons.

The number of elastic scatterings which an electron undergoes before it is slowed down to rest in the atmosphere is generally quite large. For example, with the cross sections used in BSM, one finds that the average number of collisions is 170 for an initial energy of 10 keV, 290 for 20 keV and 1060 for 100 keV. An alternative, less time-consuming, method has therefore been used in most of the calculations reported here, which is referred to as Monte Carlo Model A in BSM. This approach reduces the required computational effort through the combined use of random sampling and analytical multiple scattering theories. Each electron track to be sampled is

1

divided into a number of segments (usually not more than ~ 100) whose lengths are chosen so that the number of elastic scatterings per segment is large whereas the net multiple-scattering deflection and energy loss per segment are small.*/ The angular

---

---

deflections in successive segments are sampled from the distribution of GOUDSMIT and SAUNDERSON (1940), and the energy-losses from the distribution of LANDAU (1944) with the binding correction of BLUNCK and LEISEGANG (1950). These deflections and energy losses are then combined to construct the complete electron track. Monte Carlo Model A also includes the production and subsequent diffusion of secondary electrons, and the production, scattering and photo-electric absorption of secondary bremsstrahlung photons. The transport of bremsstrahlung photons is followed by conventional random sampling techniques (FANO, SPENCER and BERGER, 1959) involving the sampling of all successive Compton scatterings until photoelectric absorption occurs.

In order to obtain our backscattering results for initial electron energies ≤ 20 keV we have used another method, which is described in detail in BSM where it is referred to as Monte Carlo Model B. In this model all successive elastic scatterings of an electron are followed by random sampling, with use of the appropriate single-scattering cross section. The numerous inelastic collisions are lumped together and are treated in the continuous-slowing-down approximation, assuming a relation between electron energy and pathlength traveled given by stopping power theory. In this approximation, secondary knock-on electrons are not taken into

2

account.*/

For each source energy and geometry of interest, a large set of electron tracks

(typically 10,000) was simulated according to Model A or B or, in some cases, with

both. The sampled tracks were then analyzed to obtain information about various

transport phenomena including backscattering, energy deposition and electron flux

spectra. Details of some of the sampling procedures and analysis are described in

BERGER (1963) and BERGER and SELTZER (1968).

3. CROSS SECTIONS

In Monte Carlo Model A the cross section for the elastic scattering of electrons

by atoms, needed for the evaluation of the Goudsmit-Saunderson multiple-scattering

distribution, is taken from the theory of MOTT (1929) which includes spin and

relativistic effects. In Model B, applied at low energies, relativistic effects

are unimportant and the Rutherford cross section can be used. In both models, the

cross section at small angles is modified by a screening correction given by

MOLIÈRE (1947, 1948). The electron stopping power values have been taken from the

Bethe theory as formulated by ROHRLICH and CARLSON (1954).

Because of the use of the Born approximation, and because of the incomplete

treatment of atomic binding effects, the theoretical cross sections used in our

Monte Carlo program to describe interactions between electrons and the atmospheric

constituents are expected to be applicable only down to some cut-off energy, perhaps

3

comparable to the K-shell binding energies of the atoms involved. We estimate that the overall cross section uncertainty is still only 10% to 15% at 0.5 keV, but becomes greater at lower energies. We expect that the transport calculations of energy deposition will give reliable results under conditions such that the electrons have lost the predominant part of their initial energy, and have traveled a path-length equal to a large fraction of their initial range, when they reach an energy of 0.5 keV.

There is experimental evidence regarding the reliability of the calculations. It has been shown in BSM that the calculated spatial distribution of energy deposition in air is in good agreement with the results of a laboratory experiment by GRÜN (1957) with electron beams incident with energies as low as 5 keV. Comparisons with similar measurements of COHN and CALEDONIA (1970) in nitrogen indicate similarly good agreement down to 2 keV. In this paper it will be shown that the calculated backscattering coefficients for air are in agreement with experimental data down to 2 keV. There are at present no laboratory data which could be used to check the calculated electron flux spectra. It is possible that the spectral distributions are more sensitive to the cross section input than energy deposition distributions or backscattering coefficients. The electron flux spectra are therefore expected to be the most tentative of the results in this paper, and subject to revision in the light of better cross section information.*/

---

*New information on low-energy electron scattering and energy loss processes is gradually accumulating. We are beginning a new cycle of transport calculations according to Monte Carlo Model C, using data such as the semi-empirical energy loss functions of GREEN and PETERSON (1968), the inelastic electron scattering cross sections measured by OPAL, BEATY and PETERSON (1972) and calculated by OMIDVAR, KYLE and SULLIVAN (1970), and the measured elastic scattering cross sections of BROMBERG (1970) and SHYN, STOLARSKI and CARIGNAN (1972). Much work is yet needed to generate from these and similar data the comprehensive data base needed for the Monte Carlo calculations.

---

4. SCHEMATIZATION

Electrons are assumed to be incident onto the boundary of a semi-infinite air medium with kinetic energy T_0 and obliquity θ_0 (angle between the direction of incidence and the normal to the boundary plane). Electron transport is calculated as a function of the depth z_m in the medium, i.e. the mass thickness (in g cm^{-2}) measured from the boundary plane. The boundary plane is treated as non-reentrant, so that electrons (or electron-produced bremsstrahlung photons), after escaping from the medium, cannot return to it. The incident electron beam current across the boundary plane is assumed to be either monodirectional (with a fixed obliquity angle θ_0), or characterized by an angular distribution proportional to $\cos\theta_0$.

In applications to the atmosphere, the obliquity angle θ_0 (at sufficiently high magnetic latitudes) can be identified with the incident pitch angle; z_m is the atmospheric depth; the cosine-law/pitch-angle distribution corresponds to the case of an incident electron flux isotropic over the downward hemisphere (to be denoted by the abbreviation IDH). As has been shown by REES (1964a), the relation between the atmospheric depth z_m and the altitude h is given by

$$z_m = \int_h^\infty D(h) \left[\frac{4 - 3x}{4 - 4x}\right]^{1/2} dh \tag{1}$$

where

$$x = \cos^2 \lambda_m (1 + h/a), \tag{2}$$

λ_m is the geomagnetic latitude, a is the radius of the earth and D(h) is the density of the atmosphere. In the present work we have assumed that D(h) is given by the CIRA (1965) mean atmosphere for heights between 30 km and 300 km.

5. NEGLECT OF MAGNETIC MIRRORING

Electrons are deflected in the atmosphere not only as the result of multiple Coulomb scattering but also by magnetic mirroring. The combined action of both effects has been included in the calculations of WALT, McDONALD and FRANCIS (1967),

5

who solved the electron transport equation in the Fokker-Planck approximation, and in the Monte Carlo calculations of WEDDE (1970) and McENTIRE (1972). The calculations reported here do not include the effects of magnetic mirroring. The results are nevertheless applicable to atmospheric problems, provided one limits the applications to altitude no greater than, say 300 km. We have therefore assumed that the atmospheric depth $z_m = 0$ (the boundary of the semi-infinite air medium where the characteristics of the incident electron beam are specified) corresponds to an altitude of 300 km.

This assumption has practically no effect on the interpretation of the calculated multiple Coulomb scattering results, because the mass thickness of the atmosphere above 300 km is negligibly small compared to the range of the electrons at the energies of interest. The magnetic deflection angles are generally small compared to Coulomb multiple-scattering deflections for electrons starting out at 300 km. They can be estimated assuming a magnetic dipole field and using the adiabatic invariance of the quantity $\sin^2\theta/H$, where θ is the pitch angle and H the magnetic field strength. Typical pitch-angle changes are given in Table 1 for electrons that start with various initial pitch angles at altitudes of 300 or 200 km and travel down to heights of 90 or 50 km. It can be seen that in most cases the magnetic deflection angles amount to only a few degrees and become significantly greater only when the initial pitch angle approaches 70°. Moreover, the fraction of the electrons with pitch angles greater than 70° is small for an incident electron flux isotropic over the downward hemisphere.

6. ELECTRON BACKSCATTERING

The backscattering of electrons from the ionosphere was observed in rocket experiments by McDIARMID, ROSE and BUDZINSKI (1961) and in the Injun III satellite experiments of O'BRIEN (1964). According to O'Brien, approximately 10% of the electrons reaching the atmosphere are backscattered into the magnetosphere, which

is consistent with the results of our calculations. More evidence on backscattering has been obtained in an "electron echo" experiment by HENDRIKSON, McENTIRE and WINKLER (1970) in which 40-keV electrons were injected into the atmosphere from a rocket-borne accelerator at a height of 300 km at a geomagnetic latitude of 52° N, with emission pitch angles between 60° and 120°. The injected electrons traveled back and forth between the mirror point near the rocket and the conjugate southern mirror point, and several electron echos were detected for each emitted pulse. The southern conjugate mirror point was almost at sea level, so that Coulomb scattering rather than magnetic mirroring was primarily responsible for the appearance of the echos. In an analysis of this experiment, McENTIRE (1972) has made an elaborate Monte Carlo calculation which takes into account not only multiple Coulomb scattering in the atmosphere (by a method similar to our Monte Carlo Model B) but also the motion of the electrons under the action of the geomagnetic field. These calculations are reported to account quite well for many features of the observed electron echos.

Our calculations are aimed not so much toward the explanation of a particular experiment as toward the production of background information of general interest. First of all, we shall examine the validity of the multiple-scattering calculations through the comparison with laboratory experiments. Such a comparison is possible in respect to the number albedo R_N, i.e. the fraction of the incident electrons that are backscattered from a semi-infinite medium. Several authors have measured the number albedo for series of target materials with atomic numbers bracketing that of air $\left(Z_{av} = 7.4 \right)$. We have interpolated graphically with respect to atomic number and have thus obtained the experimental R_N-values shown in Fig. 1. Also shown in that figure is the calculated curve of R_N vs. the energy of incidence, T_o, for T_o between 2 keV and 2 MeV. The calculated results have an estimated statistical uncertainty (relative standard deviation) of 3%; including systematic error, the uncertainty

may be as large as 5%. The uncertainty of the experimental results is indicated in some cases, and can also be judged from the dispersion among the backscattering coefficients from different experiments. Within the combined limits of experimental and calculational error there seems to be good agreement between predicted and observed number-albedo values. The theoretical number albedo shows a systematic increase as T_o is decreased. So do the experimental values, except that some experiments indicate a leveling off at an energy $T_o \sim 2$ keV.*

---

*Calculated backscattering coefficients for air have been given previously by MAEDA (1965). His results, for $T_o = 20$ keV, are in good agreement with the present results. At lower energies his backscattering coefficients are smaller and have a different energy dependence, showing a decrease rather than an increase with decreasing T_o. These discrepancies may be related to difficulties with Maeda's electron flux calculations discussed below in Section 9.

The calculation also provided results not available from experiments, namely, the number albedo R_N and the energy albedo R_E (fraction of incident energy backscattered) as functions of the obliquity of the incident electrons. In Fig. 1, R_E is shown together with R_N for incident energies between 2 keV and 2000 keV, for perpendicular incidence ($\theta_o = 0^\circ$) and for a cosine-law source (IDH case in the atmosphere). Figs. 2a and 2b show R_N and R_E as functions of the incident obliquity angle θ_o, for incident energies of 10, 100 and 1000 keV.

We have insufficient data to give a distribution of backscattered electrons differential in energy and direction. We can only show the angular distribution regardless of energy, and the energy spectrum regardless of the direction of emergence. The dependence of these single-variable distributions on the incident energy T_o is greatly reduced if one normalizes them through division by the backscattering coefficient R_N. Normalized angular distributions $w(\theta)$ are shown in Fig. 3 for $\theta_o = 0^\circ$ and for the IDH case, in the form of universal curves which are

8

applicable for all T_o-values between 2 keV and 2 MeV. Normalized cumulative energy spectra are shown in Figs. 4a and 4b for $\theta_o = 0^o$ and the IDH case. Again the results are insensitive to the value of T_o, particularly for $T_o < 100$ keV. The dependence of the normalized cumulative energy spectra of backscattered electrons on the incident obliquity angle θ_o is shown in Figs. 5a,b and c for incident energies of 10, 100 and 1000 keV.

7. ENERGY DEPOSITION BY ELECTRONS

The basic quantity of interest is the <u>energy deposition</u> function $A(z_m)$ which is defined as the energy deposited per unit mass thickness at a depth z_m from the boundary of a semi-infinite medium. We shall assume that $A(z_m)$ is expressed in units of eV/(g cm^{-2}), and the depth z_m in g cm^{-2}. The amount of energy deposited per cm^3 in the atmosphere at an altitude h, normalized to an incident beam of 1 electron cm^{-2}, is given by $D(h)A[h(z_m)]$, where $D(h)$ is the atmospheric density, in g cm^{-3}, and where z_m and h are related by Eq(1). We shall refer to the product $D(h)A[h(z_m)]$ as the <u>altitude profile of energy deposition.</u>[*]

---

[*]The notation is the same as in BSM where the symbol ρ was used to indicate a radial spatial variable and D to indicate the density. The energy deposition function A was called penetration function in BSM.

The energy deposition function $A(z_m)$ has previously been computed in BSM with Monte Carlo Model B for electrons with incident energies between 2 keV and 20 keV. Using Monte Carlo Model A, we have now extended these calculations up to 2000 keV for the case of perpendicular incidence, and to 500 keV for the cosine-law (IDH) case. At 20 keV, the old and the new calculations are in close agreement. The accuracy of the calculated energy deposition functions is estimated to be 3% or better. As shown in BSM, there is good agreement between the calculations and experimental laboratory data in air obtained by GRÜN (1957) at ..

energies up to 54 keV. Our results are therefore also consistent with the empiri-
cal energy deposition/of REES (1963) at energies up to 300 keV, obtained by interpo-
lation and extrapolation of Grün's data. Further experimental confirmation is
available from the measurements of McLAUGHLIN and HUSSMANN (1969) at 100 and 400
keV, and the measurements of ROSENSTEIN, EISEN and SILVERMAN (1971) at 2000 keV,
in a medium (polystyrene) with an average atomic number close to that of air.

In order to minimize the dependence of the energy deposition function on the
initial electron energy T_o, it is useful to tabulate it in scaled form, by ex-
pressing depths as fractions of the initial electron range. The simplest scaling
parameter that can be used is the mean range[*] r_o, calculated by integrating

---

[*]The mean range r_o (sometimes also denoted as c.s.d.a. range because it is calcu-
lated in the continuous-slowing down approximation) is numerically equal to the
pathlength which the electron would travel if it lost energy at every point along
its trajectory at a rate equal to the mean loss given by stopping-power theory
(see, e.g. BERGER and SELTZER, 1964).

---

the reciprocal of the stopping power from energy T_o down to zero. For low values
of T_o, say below 5 keV, the mean range r_o is not very well defined because of lack
of adequate information about low-energy cross sections. In BSM this difficulty
was circumvented by using as/scaling parameter the so-called practical range[**] r_p,

---

[**]The practical range r_p is the quantity obtained by extrapolating the linear
portion of the curve of energy deposition vs. depth (see BSM); r_p depends not
only on the initial electron energy, but also on the distribution of initial
obliquity angles, and is thus different for perpendicular incidence and the IDH
case.

---

which is better defined at low energies but must be obtained from a complete trans-
port calculation. In the present work, for $T_o \geq 20$ keV, we have reverted to the use
of the mean range r_o.

The scaled energy deposition function will be found tabulated in Table 2a for
the case of perpendicular incidence, and in Table 2b for the IDH case. Each table

contains a high-energy part, consisting of the dimensionless quantity $(r_o/T_o) A(z_m)$ as a function of z_m/r_o, for $T_o \geq 20$ keV; and a low-energy part, excerpted from BSM, consisting of the dimensionless quantity $(r_p/T_o) A(z_m)$ as a function of z_m/r_p, for $T_o \leq 20$ keV. Together, the low and high-energy parts span the energy region from 2 keV to 2000 keV for perpendicular incidence, and from 2 keV to 500 keV for the IDH case. At the matching energy ($T_o = 20$ keV) the two different scaled representations give the same values for $A(z_m)$. The values of the ranges r_o and r_p, needed to interpret the data in Tables 2a and 2b, are given in Table 3.

By interpolation with respect to T_o one can readily obtain energy deposition functions and altitude profiles of energy deposition for any incident electron spectrum of interest, for example, exponential and power-exponential spectra of the form $T_o^\gamma \exp(-T_o/\alpha)$. The data in Tables 2a, 2b and 3 are given only for incident energies T_o greater than 2 keV. However, the spectra of interest may contain electrons with lower energies that make a significant contribution to the energy deposition, particularly at very high altitudes. It is possible to include the contribution from these electrons by extrapolating the scaled energy deposition function, $(r_p/T_o) A(z_m)$, and the practical range, r_p, to lower energies. A simple approximation is to assume that the scaled energy deposition function retains the shape it has at 2 keV; exploratory Monte Carlo calculations indicate that the error incurred by this assumption is probably smaller than 20% even for T_o-values as low as 0.2 keV. Extrapolation of r_p for the IDF case leads to estimated values of 4.7×10^{-6}, 1.8×10^{-6} and 6.6×10^{-7} g cm^{-2} at 1, 0.5 and 0.2 keV, respectively.

When calculating the results given below we have assumed that the exponential or power-exponential spectra extend down to $T_o = 0$. The contributions of electrons with initial energies less than 2 keV to the energy deposition are shown in Table 4 for various atmospheric depths. In Fig. 6 we give the altitude profile of energy deposition for a purely exponential spectrum ($\gamma = 0$), assuming an incident flux isotropic over the downward hemisphere and e-folding energies α between 5 keV and 200 keV. We estimate that the uncertainty of these results due to the low-energy extrapolation is $\lesssim$ 20% at 300 km, $\lesssim$ 10% at 200 km, and $\lesssim$ 5% at 150 km.

In Table 5 we give data for the case of a power-exponential spectrum $T_o^\gamma \exp(-T/\alpha)$: the height $\hat{h}$ at which the altitude profile peaks and the corresponding peak value $D(\hat{h})A[z_m(\hat{h})]$, for various α-γ combinations. All of the above results are evaluated assuming in Eq.(1) a geomagnetic latitude of 90°. The dependence of the altitude profile on the geomagnetic latitude is slight, and is indicated in Table 6 for the example of a power-exponential spectrum with $\gamma = 0.5$ and $\alpha = 10$ keV.

8. ENERGY DEPOSITION BY ELECTRON-PRODUCED BREMSSTRAHLUNG

Electron beams deposit their energy in the atmosphere not only directly but also indirectly via bremsstrahlung. The amount of bremsstrahlung energy deposited is small but significant because the photons can penetrate down to altitudes of 30 km or lower, which the primarily electrons cannot reach.

The energy deposition function for bremsstrahlung, $A_{br}(z_m)$ has been obtained by evaluating the expression

$$A_{br}(z_m) = \int_o^{T_o} \Phi_o(k,z_m,T_o)\, k\mu_{en}(k)dk \tag{3}$$

where k is the bremsstrahlung photon energy, $\Phi_o(k,z_m,T_o)$ the bremsstrahlung flux spectrum at depth z_m due to incident electrons of energy T_o, and $\mu_{en}(k)$ the photon energy absorption coefficient for air (HUBBELL, 1969). The bremsstrahlung flux spectra were taken from recent calculations (BERGER and SELTZER, 1972) for

13

the case of broad beams of electrons entering a semi-infinite medium with a cosine-law angular distribution (corresponding to the IDH case and wide-area precipitation into the atmosphere). In order to reduce the explicit dependence on T_o, we have found it useful to tabulate the quantity $A_{br}(z_m)/T_o$ as a function of the variable z_m/T_o. Such data are given in Table 7 and are sufficient to determine, by interpolation, the energy deposition by bremsstrahlung at atmospheric depths up to 20 g cm^{-2}, for incident electron energies between 20 keV and 2000 keV. By such an interpolation we have obtained altitude profiles of energy deposition by bremsstrahlung resulting from the uniform wide-area precipitation into the atmosphere of electron beams with exponential energy spectra. These results, for e-folding energies between 5 keV and 200 keV, are shown in Fig. 7.

9. ELECTRON FLUX SPECTRA

As an electron beam penetrates down into the atmosphere, the spectrum of primary electrons is shifted towards lower energies, and a buildup of low-energy secondary electrons takes place. Simple estimates of the change of the primary spectrum have been made by various authors, e.g. REES(1964b) and STOLARSKI (1968) who implicitly assumed that the spectrum at any depth z_m is monoenergetic and con-centrated at an energy

$$T(z_m) = T_o - \int_o^{z_m} A(z'_m)dz'_m \ , \tag{4}$$

where $A(z_m)$ is the energy deposition function. This is equivalent to assuming that the electrons move along straight lines and lose energy at a rate per unit pathlength equal to $A(z_m)$.

The spectrum actually is not monoenergetic but rather broad because of the occurrence of two types of fluctuations.

14

First, the electrons do not really travel in straight lines, because of multiple-scattering angular deflections, so that the pathlength traveled down to depth z_m is a stochastic quantity. Second, even for a given pathlength, the actual energy loss fluctuates around the mean given by the continuous-slowing-down approximation. Both types of fluctuations - pathlength and energy-loss straggling - have been taken into account in the present calculations which also include the buildup of secondary electrons.

We have calculated the spectrum only down to a cut-off energy Δ, which was chosen to be 5% of the initial energy T_o [*], and have also computed the average

___

[*] For the lowest source energy treated, 2 keV, the cut-off energy Δ was $0.1\ T_o = 200$ eV.

___

number of electrons per unit depth, $n_\Delta(z_m)$, that reach an energy Δ . The relation between the flux spectrum $F(T, z_m)$ and the energy deposition function $A(z_m)$ is given by

$$A(z_m) = \Delta \cdot n_\Delta(z_m) + \int_\Delta^{T_o} F(T, z_m) L_\Delta(T) dT \quad , \tag{5}$$

where $F(T, z_m)$, in MeV^{-1}, is the spectrum [**] of primary plus secondary electrons, and

___

[**] The electron flux differential in energy and direction is defined as the number of electrons per unit energy and solid angle that cross a unit area perpendicular to the direction of motion. The spectrum $F(T, z_m)$ is obtained from the doubly differential flux distribution by integrating over all directions of motion, and can thus be interpreted as the distribution with respect to energy of electrons crossing a small spherical probe at depth z_m.

___

where $L_\Delta(T)$ is the restricted stopping power. $L_\Delta(T)$ includes energy losses from electron interactions resulting in atomic excitations or in ionizing events in which secondary electrons with energy smaller than Δ are released; it is less than or equal to the ordinary stopping power and can be computed with the use of Eqs(22-23) of BERGER and SELTZER (1964).

Comparison with a Previous Calculation. A Monte Carlo calculation of electron

flux spectra, somewhat similar in scope to the present work, was done by MAEDA

(1965) whose results were fitted to analytical expressions by MAEDA and AIKIN

(1968) and used by REES (1969) for the analysis of satellite and rocket measure-

ments of auroral electrons. Recently, SHEMANSKY, DONAHUE and ZIPF (1972) have

studied the relation between the emission lines from excited nitrogen molecules

and the energy flux spectrum of the auroral electron responsible for the excita-

tion. Their analysis led them to the conclusion that Maeda's spectra are deficient

in low-energy degraded primary electrons, and that the rate at which electrons
                                                              five
from these spectra would ionize the atmosphere is up to / times smaller than the

integrated ionization rate inherent in the incident electron flux. The present

result supports the conclusions of Shemansky et al.

       a
For/detailed comparison we have chosen the case of 20-keV electrons incident

perpendicularly. Fig. 8 shows the electron spectrum $F(T,z_m)$ calculated with our

Monte Carlo Model A and the corresponding quantity, denoted as "differential energy

spectrum" given earlier by MAEDA (1965). In Fig. 9 we show the distribution function

$n_\Delta(z_m)$ also obtained in our Monte Carlo calculation. When $F(T,z_m)$ and $n_\Delta(z_m)$ are

inserted into the right-hand side of Eq(5), the energy deposition thus obtained is

in agreement to within 5% or better with the value of the energy deposition function

$A(z_m)$ from Table 2a.[*/] This shows that our energy deposition and flux spectrum

---

[*]In the case under discussion, the contribution to energy deposition from electrons
with energies $\leq \Delta$ (not treated explicitly in the Monte Carlo calculation) is
relatively minor, and can be approximated by the formula

$$[\Delta \cdot n_\Delta(z_m)/A(z_m)] = 0.064 + 0.122 \ (z_m/r_o).$$

---

calculations are indeed consistent in the sense that energy is conserved.

It can be seen from Fig. 8 that Maeda's "differential spectrum" is lower than $F(T,z_m)$ at all three depths shown, and that the discrepancy becomes more marked at the lower spectral energies. When a weighted integral[*] is taken over "differential spectrum" the resulting energy deposition values are smaller than $A(z_m)$ from Table 2a by factors ranging from 2.4 to 5.5. This is consistent with the energy (or ionization)-content discrepancy noted by Shemansky et al for an incident electron spectrum with a $T_o^{1.25}$ power law.

---

[*]The distribution $n_\Delta(z_m)$ is not available from Maeda's work. We have therefore omitted the first term on the right-hand side of Eq(5) and have compensated for this by using as weighting factor the total stopping power $L(T)$ rather than the restricted stopping power $L_\Delta(T)$. The error incurred thereby is estimated to be small compared to the discrepancies by factors up to 5 which are being investigated.

We have attempted, but failed, to account completely for this discrepancy, but were at least able to reduce it considerably, by analyzing what quantity was actually computed in Maeda's work. The following points were considered:

(1) The Monte Carlo program for simulating electron tracks used by Maeda was based on the procedures of BERGER (1963) and was thus an ancestor of the Monte Carlo Model A used in the present work. The early version lacked certain refinements but was not essentially different from the current version.

(2) The early version of the program included only primary electrons. However, it can be seen from Fig. 8 that for the 20-keV source the contribution of secondary electrons becomes significant only at spectral energies $\lesssim 4$ keV.

(3) The early version of the program provided as output not the electron flux spectrum in a semi-infinite medium, but the electron current[**] transmitted

---

[**]In the Monte Carlo calculation the transmitted current is estimated by counting the electron tracks that cross a unit area of the exit surface of the slab target. Once the electrons have left the slab they are not allowed to return to it, so that the exit surface is crossed at most once. The flux in a semi-infinite medium is estimating by computing the lengths of electron tracks in many thin layers of the medium parallel to the boundary plane. Each layer of the medium is allowed to be crossed repeatedly by the same electron, in the direction away from or toward the boundary plane.

---

through a slab target. This current, denoted by Maeda as "differential energy spectrum" differs both conceptually and numerically from the electron flux spectrum as defined above.

In order to determine whether the discrepancy could be accounted for by the substitution of current for flux in Maeda's work, we have made model studies in which both quantities were calculated from the same set of sampled electron Monte Carlo histories. A typical set of results is shown in Fig. 10 which gives the total flux (denoted in this instance as $F_{4\pi}(T,z_m)$), the contribution to the flux from electrons moving in the direction of increasing depth, $F_{2\pi}(T,z_m)$, and the current of electrons transmitted through a slab target of thickness z_m, $J(T,z_m)$. Of these three distributions, $J(T,z_m)$ is closest to Maeda's "differential energy spectrum", but is still higher by a factor of 2 or more.

Some New Results. We would like to repeat that the spectra given here are preliminary, because they are calculated with oversimplified cross sections and by applying Monte Carlo Model A at lower energies than is, strictly speaking, permissible. Furthermore it would be desirable to extend the spectra below the cut-off Δ of the present work (5% of T_o). In any case, we have verified that the energy content of the spectra is correct, in the sense that the relation between energy deposition and integrated spectra according to Eq(5) is satisfied (to within 5% at 20 keV, 5-10% at 10 and 5 keV, and 10-20% at 2 keV).*

---

*The decreasing accuracy at low source energies results from numerical approximations of the Monte Carlo scheme. At 2 keV we have found it necessary to use the total rather than the restricted stopping power in Eq(5) to get the desired energy balance, corresponding to the fact that the Monte Carlo treatment at extremely low energies approaches the continuous-slowing-down approximation.

The results to be shown indicate that the dependence of the electron flux spectra on the initial energy T_o and the depth z_m can be simplified considerably by certain scaling procedures. The dependence on T_o can be minimized by expressing the spectra as functions of the ratio T/T_o, where T is the spectral energy. The dependence on the depth z_m can be reduced by plotting instead of $F(T,z_m)$ the

18

dimensionless quantity $[T_o/r_p A(z_m)] F(T_o z_m)$ vs T/T_o, where r_p is the practical range. The results in the following figures are normalized to one incident electron.

The residual dependence of the scaled flux spectra on T_o is illustrated in Fig. 11, for T_o between 2 and 20 keV, and can be seen to be rather small. The flux spectra shown in the remaining figures all pertain to electrons incident with energy T_o = 10 keV. The change of the spectral shape with increasing depth is illustrated by Fig. 12. As expected, there is a spectral peak at or near T_o, due to primary electrons which have lost only a small part of their energy. This peak disappears with increasing depth. There is also a low-energy component in the spectra, contributed (a) by primary electrons that have lost most of their energy in the course of traveling deep into the medium and were eventually turned around; (b) by low-energy secondary electrons resulting from inelastic collisions. Fig. 13 separates the flux spectra into the contributions from electrons traveling in the direction of increasing depth (DOWN) or decreasing depth (UP). At shallow depths one can distinguish three spectral regions. Near T_o, downward-directed primary electrons predominate; at somewhat lower energies, upward-directed electrons predominate, and at low energies the number of upward and downward directed electrons is approximately equal, indicating that the low-energy flux component is more or less isotropic. At great depths the downward-directed flux exceeds the the upward-directed flux, except at very low energies where the two components remain approximately equal. Finally, Fig. 14 shows the dependence of the flux spectra on the direction of incidence, θ_o. This dependence is more pronounced for spectral energies near T_o than at low energies, because the low-energy electrons have undergone so many interactions that they have "forgotten" their initial direction.

REFERENCES

BERGER M.J. — 1963 — Methods in Computational Physics, Vol. 1, pp. 135-215. Academic Press, New York

BERGER M. J. — 1972 — Proc. of Third Symposium on Microdosimetry. EURATOM Document EUR 4810 d-f-e. ed. H.G. Ebert.

BERGER M.J. and SELTZER S.M. — 1964 — Tables of Energy Losses and Ranges of Electrons and Positrons, NASA Spec. Publ. No. 3012

BERGER M.J. and SELTZER S.M. — 1968 — Protection Against Space Radiation, pp. 285-322. NASA Spec. Publ. No. 169.

BERGER M.J. and SELTZER S.M. — 1972 — J. Atmosph. Terr. Phys. $\underline{34}$, 85.

BERGER M.J., SELTZER S.M. and MAEDA K. — 1970 — J. Atmosph. Terr. Phys. $\underline{32}$, 1015.

BISHOP H.E. — 1966 — X-ray Optics and Microanalysis, p.153. Hermann, Paris.

BLUNCK, O. and LEISEGANG — 1950 — Z. Physik $\underline{128}$, 500.

BROMBERG J.P. — 1970 — J. Chem. Phys. $\underline{52}$, 1242

CIRA — 1965 — COSPAR International Reference Atmosphere. North-Holland, Amsterdam.

COHN A. and CALEDONIA G. — 1970 — J. Appl. Phys. $\underline{41}$, 3767.

FANO U., SPENCER L.V. and BERGER M.J. — 1959 — Penetration and Diffusion of X-Rays, pp. 660-817. Handbuch der Physik, ed. S. Flugge, Vol. 38/II. Springer-Verlag, Berlin.

GLAZUNOV P.Ya. and GICLYA V.G. — 1964 — Dokl. Akad. Nauk. USSR $\underline{159}$, 632.

GOUDSMIT S. and SAUNDERSON J.L. — 1940 — Phys. Rev. $\underline{57}$, 24.

GREEN A.E.S. and PETERSON L.R. — 1968 — J. Geophys. Res. Space Phys. $\underline{73}$, 233

GRÜN A.E. — 1957 — Z. Naturf. $\underline{12a}$, 89.

HEINRICH K.F.J. — 1966 — X-Ray Optics and Microanalysis, p.159 Hermann, Paris.

HENDRICKSON R.A., McENTIRE R.W. and WINCKLER J.R. — 1971 — Nature $\underline{230}$, 546.

LANDAU L. — 1944 — J. Phys. USSR $\underline{8}$, 201.

MAEDA K. — 1965 — J. Atmosph. and Terr. Phys. $\underline{27}$, 259.

MAEDA K. and AIKIN A.C. — 1968 — Planet. Space Sci $\underline{16}$, 371.

McDIARMID J.B., ROSE D.C. and BUDZINSKI E. — 1961 — Can. J. Phys. $\underline{39}$, 1888.

McLAUGHLIN W.L. and HUSSMANN E.K. — 1969 — Large Radiation Sources for Industrial Processes, pp. 579-590. Int. Atomic Energy Agency Pub. IAEA-SM-123/43.

MOLIÈRE G. — 1947 — Z. Naturf. $\underline{2a}$, 133.

MOLIÈRE G. — 1948 — Z. Naturf. $\underline{3a}$, 78.

MOTT N.F. — 1929 — Proc. R. Soc. A$\underline{124}$, 425.

O'BRIEN D.J. — 1964 — J. Geophys. Res. $\underline{69}$, 13.

OMIDVAR K., KYLE H.L. and SULLIVAN E.C. — 1972 — Phys. Rev. A $\underline{5}$, 1174.

OPAL C.B., BEATY E.C. and PETERSON W.K. — 1972 — Atomic Data $\underline{4}$, 209.

PALLUEL P. — 1947 — C.R.Acad. Sci. Par. $\underline{224}$, 1492.

REES M.H. — 1963 — Planet.Space Sci. $\underline{11}$, 1209

REES M.H. — 1964 — Planet. Spac. Sci. $\underline{12}$, 722.

REES M.H.	1964	Planet. Space Sci. 12, 1093.
REES M.H.	1969	Space Sci. Rev. 10, 413.
ROHRLICH F. and CARLSON B.C.	1954	Phys. Rev. 93, 38.
ROSENSTEIN M., EISEN H. and SILVERMAN, J.	1972	J. Appl. Phys. 43, 3191
SALDICK J. and ALLEN A.J.	1954	J. Chem. Phys. 22, 1777.
SHEMANSKY D.E., DONAHUE T.M. and SIPF E.C., Jr.	1972	Planet. Space Sci. 20, 905.
SHYN T.W., STOLARSKI R.S. and CARIGNAN G.R.	1972	Phys. Rev. A 6, 1002.
STERNGLASS E.J.	1954	Phys. Rev. 95, 345.
STOLARSKI R.S.	1968	Planet. Space Sci. 16, 1265.
TRUMP J.G. and VAN DE GRAAFF R.J.	1949	Phys. Rev. 75, 44.
VERDIER P. and ARNAL F.	1968	C.R. Acad. Sci. Par. 267, 1443.
WALT M., MACDONALD W.M. and FRANCIS W.E.	1967	Physics of the Magnetosphere, pp. 534-555, ed. by R. L. Carovillano et al, Reidel, Dordrecht, Holland.
WEDDE T.	1970	Norwegian Defence Res. Estab., Internal Report E-162.
WEINRYB E. and PHILIBERT J.	1964	C.R.Acad. Sci. Par. 258, 4538.
WRIGHT K.A. and TRUMP J.G.	1962	J. Appl. Phys. 33, 687.

Reference is also made to the following unpublished material:

McENTIRE R.W.	1972	The electron echo experiment - A comparison between the observed and predicted trajectories for electrons artificially injected into the magnetosphere. University of Minnesota School of Physics and Astronomy, Cosmic Physics Tech. Rep. No. 159. Also, Ph.D. Dissertation, Univ. of Minnesota.

θ_o (deg)	$\Delta\theta$, deg				$P(\theta_o)$ (%)
	$h_o = 300$ km, $h_1 = 50$ km	$h_o = 200$ km, $h_1 = 50$ km	$h_o = 300$ km, $h_1 = 90$ km	$h_o = 200$ km, $h_1 = 90$ km	
0	0.0	0.0	0.0	0.0	100.0
10	0.6	0.5	0.5	0.3	97.0
20	1.2	1.0	1.0	0.5	88.3
30	2.0	1.6	1.6	0.9	75.0
40	2.9	2.3	2.4	1.3	58.7
50	4.2	3.4	3.5	1.8	41.3
60	6.5	5.1	5.3	2.7	25.0
70	14.4	9.8	10.4	4.6	11.7
72	--	12.9	--	5.3	9.5
75	--	--	--	7.2	6.7

Table 1. Change of pitch angle, $\Delta\theta$, due to the action of the geomagnetic field, for electrons with initial pitch angle θ_o traveling from height h_o to height h_1. $P(\theta_o)$ is the percentage of electrons in a cosine-law distribution (IDH case) that have initial pitch-angles greater than θ_o.

z_m/r_p	$(r_p/T_o)\ A(z_m)$				z_m/r_o	$(r_o/T_o)\ A(z_m)$						
	T_o, keV					T_o, keV						
	2	5	10	20		20	50	100	200	500	1000	2000
0.0	0.68	0.62	0.61	0.61	0.0	0.71	0.71	0.72	0.73	0.78	0.82	0.86
0.1	0.97	0.89	0.89	0.89	0.1	1.07	1.05	1.05	1.05	1.06	1.08	1.05
0.2	1.17	1.10	1.12	1.13	0.2	1.38	1.38	1.38	1.38	1.38	1.36	1.22
0.3	1.29	1.25	1.28	1.28	0.3	1.55	1.57	1.59	1.60	1.60	1.57	1.49
0.4	1.32	1.31	1.33	1.33	0.4	1.55	1.59	1.61	1.61	1.60	1.59	1.57
0.5	1.25	1.28	1.31	1.29	0.5	1.38	1.41	1.43	1.44	1.45	1.46	1.47
0.6	1.09	1.13	1.16	1.15	0.6	1.08	1.11	1.12	1.13	1.14	1.15	1.15
0.7	0.87	0.91	0.89	0.93	0.7	0.67	0.69	0.70	0.71	0.73	0.75	0.79
0.8	0.58	0.60	0.59	0.63	0.8	0.31	0.31	0.32	0.32	0.33	0.34	0.40
0.9	0.31	0.34	0.34	0.34	0.9	0.12	0.10	0.09	0.09	0.08	0.09	0.11
1.0	0.15	0.18	0.16	0.16	1.0	0.04	0.03	0.02	0.01	0.01	0.01	0.01

Table 2a. Scaled energy deposition function, for the case of a perpendicularly incident electron flux.

	(r_p/T_o) $A(z_m)$					(r_o/T_o) $A(z_m)$				
z_m/r_p	T_o, keV				z_m/r_o	T_o, keV				
	2	5	10	20		20	50	100	200	500
0.0	1.34	1.28	1.27	1.28	0.0	1.61	1.62	1.64	1.70	1.76
0.1	1.29	1.25	1.24	1.25	0.1	1.56	1.58	1.60	1.62	1.64
0.2	1.22	1.21	1.21	1.21	0.2	1.50	1.52	1.52	1.51	1.50
0.3	1.14	1.13	1.14	1.15	0.3	1.38	1.39	1.39	1.38	1.36
0.4	1.03	1.03	1.05	1.07	0.4	1.17	1.18	1.19	1.19	1.19
0.5	0.89	0.91	0.93	0.94	0.5	0.90	0.92	0.93	0.95	0.98
0.6	0.72	0.76	0.78	0.77	0.6	0.60	0.60	0.61	0.64	0.69
0.7	0.54	0.57	0.60	0.57	0.7	0.32	0.32	0.33	0.34	0.37
0.8	0.37	0.40	0.40	0.39	0.8	0.13	0.12	0.11	0.12	0.15
0.9	0.24	0.25	0.23	0.23	0.9	0.04	0.04	0.03	0.03	0.02
1.0	0.13	0.13	0.11	0.12	1.0	0.01	0.01	0.01	0.00	0.00

Table 2b. Scaled energy deposition function, for the case of an
incident electron flux isotropic over the downward
hemisphere.

T_o (keV)	r_o (g cm^{-2})	a/ r_p (g cm^{-2})	b/ r_p (g cm^{-2})
2	1.86(-5)	1.52(-5)	1.40(-5)
5	8.73(-5)	7.19(-5)	6.65(-5)
10	2.91(-4)	2.48(-4)	2.30(-4)
20	9.82(-4)	8.45(-4)	7.83(-4)
50	4.92(-3)		
100	1.63(-2)		
200	5.09(-2)		
500	2.00(-1)		
1000	4.91(-1)		
2000	1.08		

a/ For perpendicular incidence

b/ For the IDH case

Table 3. Mean range, r_o, and practical range, r_p, for electrons in air.

z_m (g cm^{-2})	h (km)	Percent Contribution	
		α = 5 keV	α = 50 keV
0	300	63	29
10^{-6}	194.6	49	19
2×10^{-6}	173.3	40	15
5×10^{-6}	149.8	21	7
10^{-5}	135.7	7	2

Table 4. Estimated contribution of electrons with initial energies $T_o < 2$ keV to the energy deposition at various atmospheric depths. The incident electron flux is assumed to be isotropic over the downward hemisphere with an exponential energy spectrum proportional to exp $(-T_o/\alpha)$.

Table 5. Height $\hat{h}$ at which the altitude profile of energy deposition peaks, and the corresponding value $D(\hat{h})A(\hat{h})$ of the altitude profile, for the case of an incident electron flux isotropic over the downward hemisphere with a power-exponential energy spectrum proportional to $T_o^\gamma \exp(-T_o/\alpha)$. Assumed geomagnetic latitude is $\lambda_m = 90^o$.

α (keV)	height $\hat{h}$, km				
	$\alpha\gamma = 0$	2	5	10	20 keV
5	108	106	104	100	96
10	100	100	98	96	93
20	93	93	92	91	90
50	85	85	85	84	83
100	80	80	80	79	79
200	73	73	73	73	73

Altitude profile of energy deposition, $D(\hat{h})A(\hat{h})$, eV/cm

α (keV)	$\alpha\gamma = 0$	2	5	10	20 keV
5	1.29(-3)	2.05(-3)	3.37(-3)	6.07(-3)	1.22(-2)
10	3.14	3.98	5.33	7.82	1.36
20	7.01	7.93	9.35	1.19(-2)	1.74
50	1.91(-2)	2.00(-2)	2.14(-2)	2.38	2.89
100	3.93	4.02	4.15	4.38	4.84
200	7.56	7.64	7.77	7.99	8.43

Table 6. Dependence of the altitude profile of energy deposition, $D(h)A(h)$, on the geomagnetic latitude λ_m, for the case of an incident electron flux isotropic over the downward hemisphere with a power-exponential energy spectrum proportional to $T_o^{\gamma} \exp(-T_o/\alpha)$, with $\gamma = 0.5$ and $\alpha = 10$ keV. $D(h)A(h)$ is given in units of eV/cm^3 / per incident electron/cm^2. Also shown is the height $\hat{h}$ at which the altitude profile peaks.

λ_m / h, km	90°	75°	60°	45°	30°	15°
200	1.73(-5)	1.73(-5)	1.73(-5)	1.72(-5)	1.70(-5)	1.60(-5)
180	3.43	3.43	3.42	3.40	3.35	3.09
160	7.79	7.78	7.75	7.68	7.50	6.75
150	1.26(-4)	1.25(-4)	1.25(-4)	1.24(-4)	1.20(-4)	1.06(-4)
140	2.17	2.17	2.15	2.13	2.05	1.77
130	4.20	4.19	4.16	4.09	3.91	3.26
120	9.93	9.90	9.80	9.57	9.00	7.07
110	2.72(-3)	2.71(-3)	2.67(-3)	2.57(-3)	2.34(-3)	1.61(-3)
100	5.23	5.18	5.03	4.67	3.87	1.89
90	2.80	2.75	2.56	2.17	1.40	2.89(-4)
85	6.15(-4)	5.96(-4)	5.33(-4)	4.10(-4)	2.13(-4)	1.75(-5)
80	3.33(-5)	3.17(-5)	2.63(-5)	1.63(-5)	4.61(-6)	-
$\hat{h}$ (km)	98	98	98	99	100	103

z/T_o	T_o, keV						
g cm^{-2}keV^{-1}	20	50	100	200	500	1000	2000
1.0(-7)	3.1(-4)	5.8(-4)	7.0(-4)	5.7(-4)	4.9(-4)	4.1(-4)	4.1(-4)
1.0(-6)	3.1	6.0	7.0	5.8	5.0	4.2	4.2
2.0	3.1	6.1	7.0	5.8	5.0	4.3	4.4
4.0	3.1	6.2	7.1	5.8	5.1	4.4	4.6
1.0(-5)	3.2	6.5	7.2	6.1	5.2	4.8	5.0
2.0	2.9	6.8	7.5	6.5	5.6	5.2	5.7
4.0	2.5	6.4	7.9	7.0	6.2	5.8	6.7
1.0(-4)	2.1	5.0	6.8	7.1	6.8	6.6	7.8
2.0	1.8	4.1	5.1	5.4	6.2	6.7	7.9
4.0	1.5	3.2	4.0	3.8	4.2	4.9	6.3
1.0(-3)	1.1	2.3	2.6	2.3	2.4	2.8	4.0
2.0	8.3(-5)	1.6	1.7	1.5	1.5	2.0	2.9
4.0	5.8	1.0	1.0	8.8(-5)	9.9(-5)	1.4	1.9
1.0(-2)	2.8	4.6(-5)	4.5(-5)	4.3	5.3	6.4(-5)	5.8(-5)
2.0	1.2	2.1	2.3	2.4	2.6	2.4	
4.0	3.8(-6)	8.5(-6)	1.1	1.1	7.6(-6)		
1.0(-1)	4.0(-7)	1.9	2.6(-6)	2.0(-6)			
2.0	2.6(-8)	3.7(-7)	5.4(-7)				
4.0	7.5(-11)	2.4(-8)					

Table 7. Energy deposition function for bremsstrahlu for the case of uniform wide-area precipitation of an electron flux isotropic over the down-ward hemisphere. The quantity given is $A_{br}(z_m)/T_o$, in units of cm^2 g^{-1}. Numbers in parentheses indicate powers of ten.

Fig. 1. Backscattering coefficients R_N (number albedo) and R_E (energy albedo)
for monoenergetic electrons incident on a semi-infinite air medium.
The calculated coefficients are for perpendicular incidence ($\theta_o = 0^o$)
or for an incident flux isotropic over the downward hemisphere (IDH).
The experimental values of R_N are for perpendicular incidence and have
been obtained by interpolating to atomic number $Z = 7.4$ the data of
the following authors:

    B: BISHOP (1966); H: HEINRICH (1966); WP: WEINRYB and
PHILIBERT (1964); TV: TRUMP and VAN DE GRAAFF (1949);
SA: SALDICK and ALLEN (1954); WT: WRIGHT and TRUMP (1962);
GG: GLAZUNOV and GUGLYA (1964); S: STERNGLASS (1954);
P: PALLUEL (1947); VA: VERDIER and ARNAL (1968).

Fig. 2. Backscattering of monoenergetic electrons from a semi-infinite air
medium, as a function of the incident obliquity angle θ_o.

    a. Number albedo, R_N

    b. Energy albedo, R_E

Fig. 3.   Angular distribution $W(\theta)$ of the current of backscattered
electrons emerging from a semi-infinite air medium. The distributions
shown are normalized to unity over a 2π-solid angle.

Fig. 4. Cumulative energy spectra of electrons backscattered from a semi-infinite
air medium. The curves show, as a function of the incident energy T_o,
the fraction of the backscattered electrons that have energy T greater
than $0.2\ T_o$, $0.4\ T_o$, $0.6\ T_o$ or $0.8\ T_o$.

    a. Perpendicular incidence, $\theta_o = 0^o$

    b. Incident flux isotropic over downward hemisphere, θ_o:IDH.

Fig. 5. Cumulative energy spectra of electrons backscattered from a semi-infinite
air medium. The curves show, as a function of the incident obliquity
angle θ_o, the fraction of the backscattered electrons with energy T greater
than $0.2\ T_o$, $0.4\ T_o$, $0.6\ T_o$ or $0.8\ T_o$, where T_o is the incident energy.

    a. $T_o = 10$ keV   b. $T_o = 100$ keV   c. $T_o = 1000$ keV

Fig. 6. Altitude profile of energy deposition in the atmosphere, for an incident electron flux isotropic over the downward hemisphere with an exponential energy spectrum $\frac{1}{\alpha} \exp(-T_o/\alpha)$. The relation between atmospheric depth and altitude is assumed to be that given by the CIRA (1965) Mean Atmosphere at geomagnetic latitude $\lambda_m = 90^o$. Results are normalized to one incident electron/cm^2.

Fig. 7. Altitude profile of energy deposition by electron-produced bremsstrahlung in the atmosphere, for the case of wide-area precipitation of an electron flux incident isotropically over the downward hemisphere with an exponential spectrum $\frac{1}{\alpha} \exp(-T_o/\alpha)$. The relation between atmospheric depth and altitude is assumed to be that given by the CIRA (1965) Mean Atmosphere at geomagnetic latitude $\lambda_m = 90^o$. Results are normalized to one incident electron/cm^2. Dashed portions of curves are extrapolations.

Fig. 8. Comparison of the energy flux spectrum $F(T,z_m)$ with Maeda's "differential energy distribution", for 20-keV electrons incident perpendicularly on an air medium. The dotted curves indicate the contribution to $F(T,z_m)$ from degraded primary electrons.

Fig. 9. Depth distribution of electrons at cut-off energy Δ. The ordinate is the dimensionless quantity $r_o \, n_\Delta(z_m)$, where $n_\Delta(z_m)$ is the number of electrons per unit depth whose energy falls below Δ. P and S indicate primary and secondary electrons, respectively. The normalization corresponds to one incident primary electron.

Fig.10. Comparison of various spectral distributions, at a depth $z_m = 0.5\ r_o$, for 20-keV electrons incident perpendicularly on an air medium.

$F_{4\pi}(T,z_m)$: total flux spectrum

$F_{2\pi}(T,z_m)$: contribution to total flux spectrum from electrons moving in the direction of increasing depth

$J(T,z_m)$: spectrum of the current of electrons transmitted through a slab target with a thickness equal to z_m.

Fig.11. Dependence of the electron flux spectrum $F(T,z_m)$ on the incident energy T_o.

Fig. 12. Dependence of the electron flux spectrum on the depth z_m, for electrons

incident with an energy of 10 keV.

Perpendicular incidence; $r_p = 2.48 \times 10^{-4}$ g cm^{-2}

Curve	1	2	3	4	5	6	7
Depth, z_m/r_p	0.03	0.20	0.37	0.54	0.70	0.87	1.04

Incident flux isotropic over the downward hemisphere;

$r_p = 2.30 \times 10^{-4}$ g cm^{-2}

Curve	1	2	3	4	5	6	7
Depth, z_m/r_p	0.03	0.21	0.40	0.58	0.76	0.94	1.12

Fig. 13. Directional characteristics of the electron flux spectrum, for electrons

incident with an energy of 10 keV. The curves labelled DOWN and UP

represent the contributions from electrons moving in the direction of

increasing and decreasing depth, respectively. The curve marked TOTAL is

the sum of DOWN and UP.

Fig. 14. Dependence of the flux spectrum $F(T, z_m)$ on the obliquity (pitch angle) θ_o

of the incident electrons, for an incident electron energy of 10 keV;

the scaling parameter r_p in this figure is the practical range for the

case of perpendicular incidence.
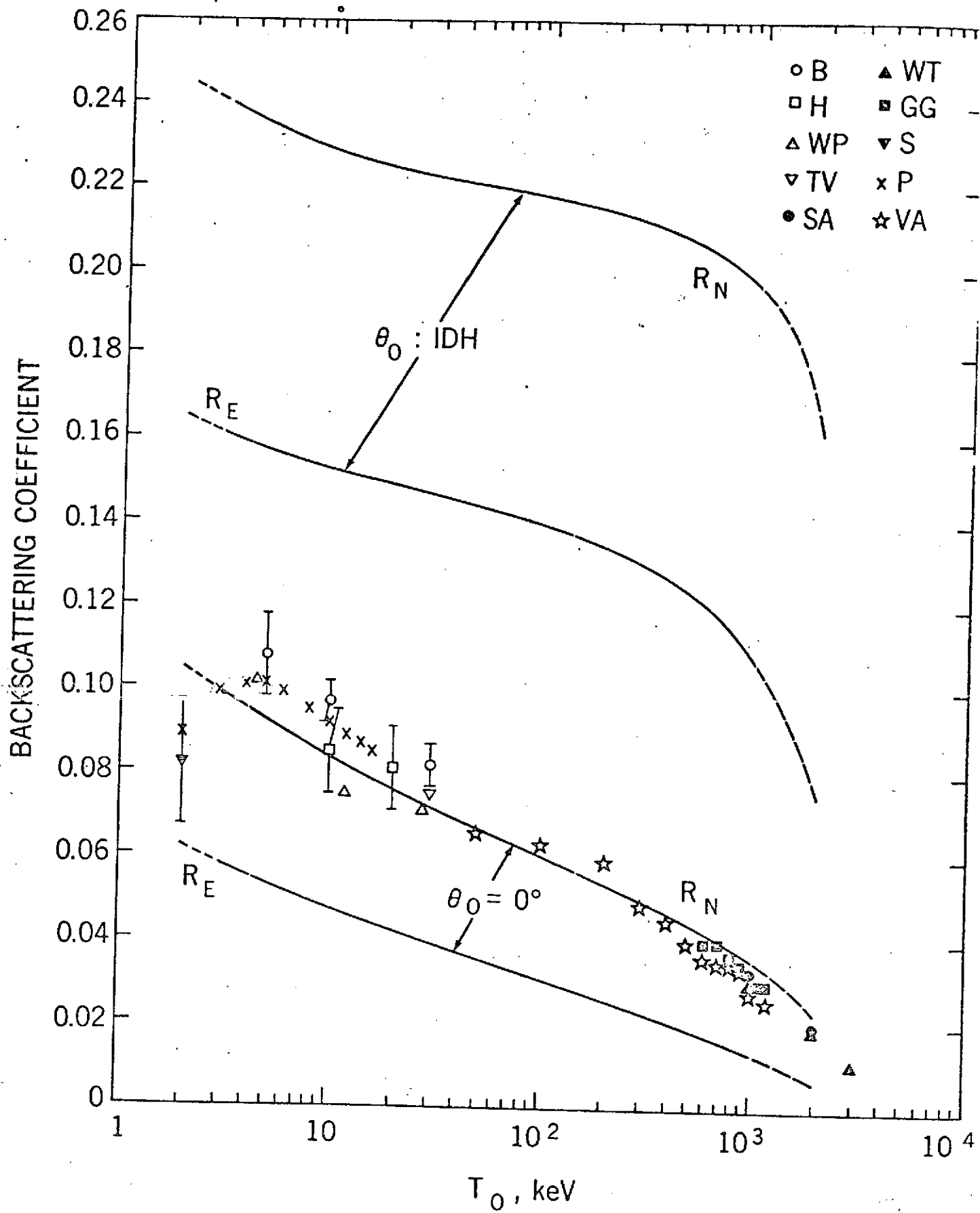
Fig. 1
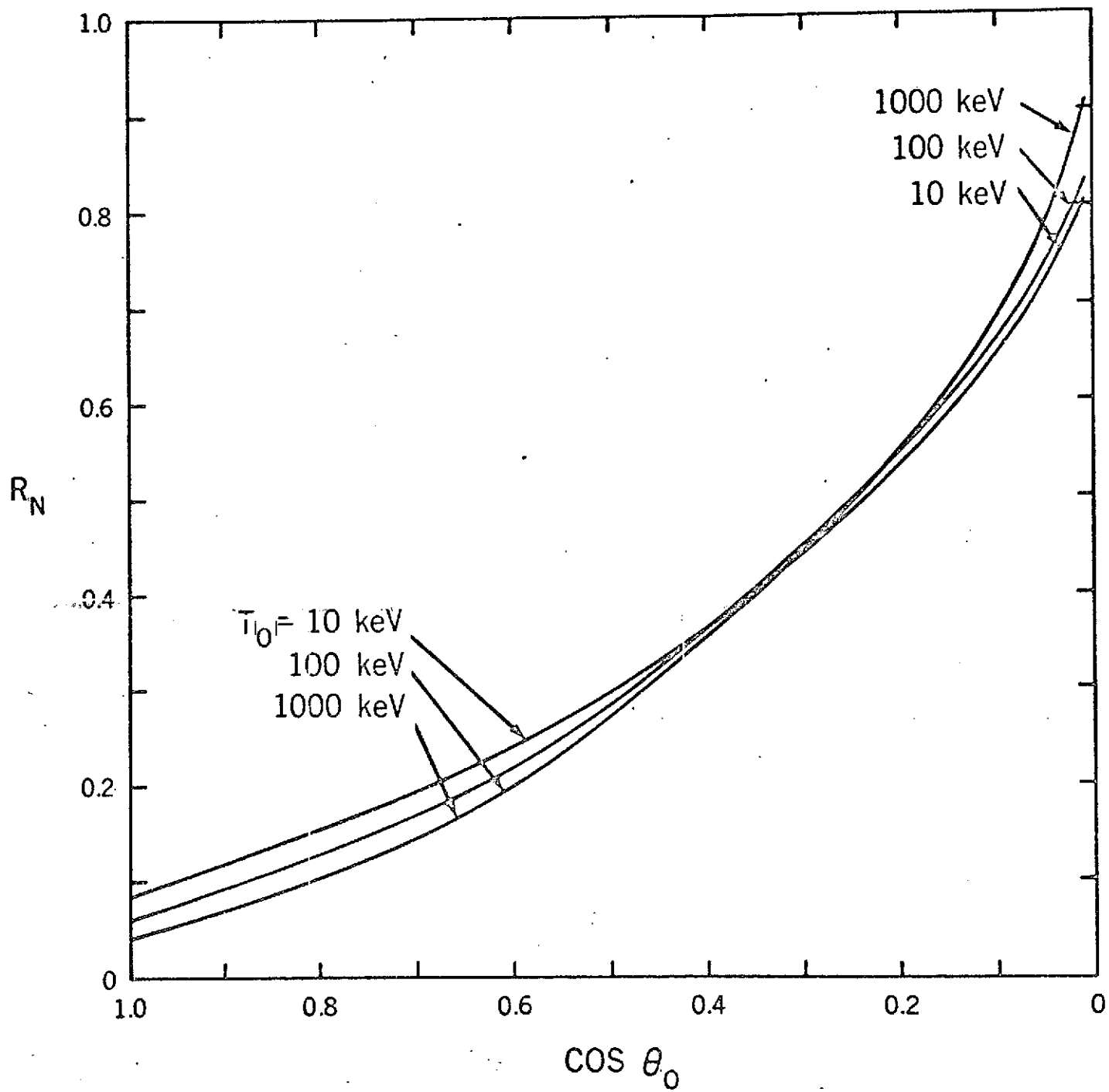
Fig. 2a
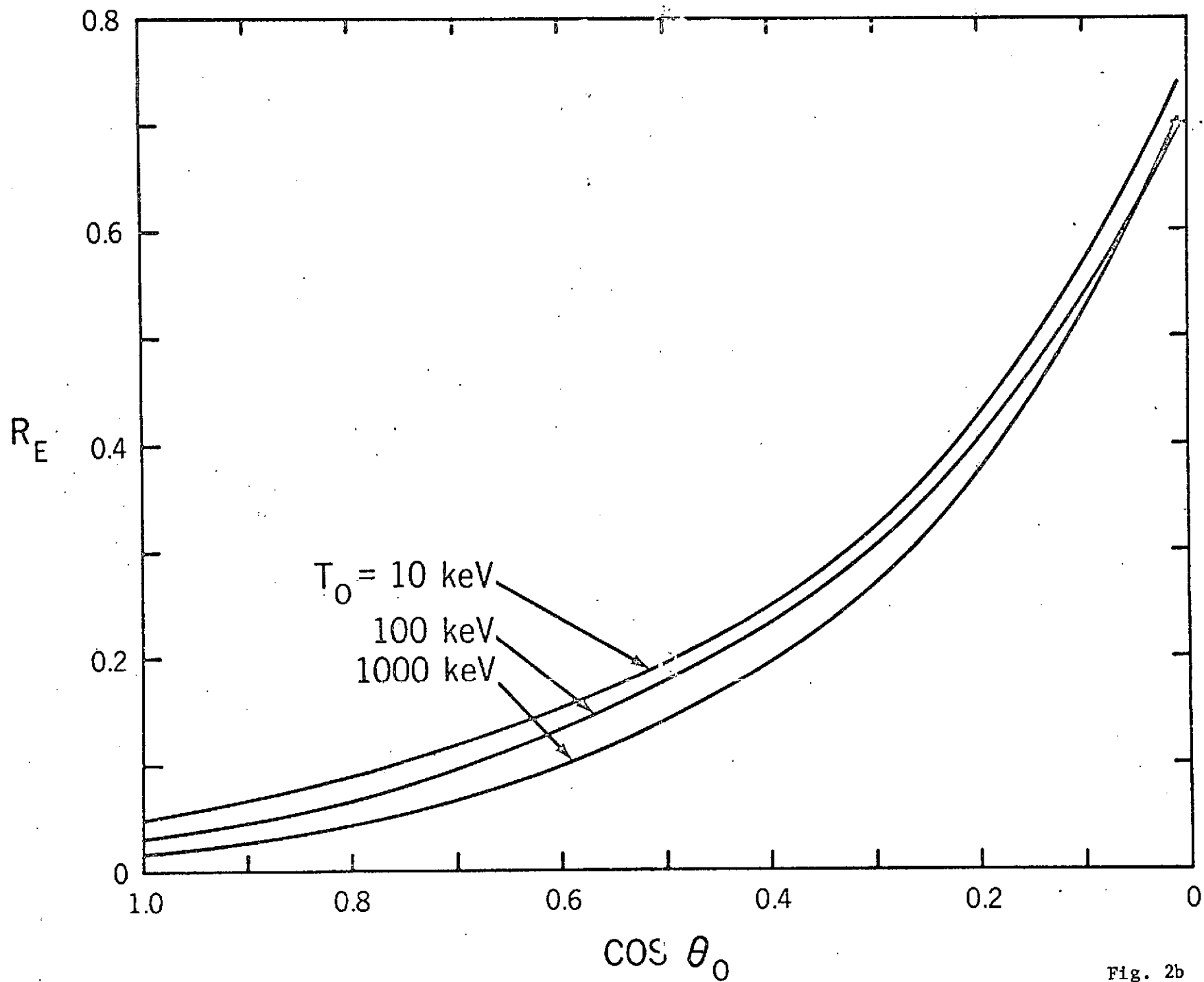
Fig. 2b
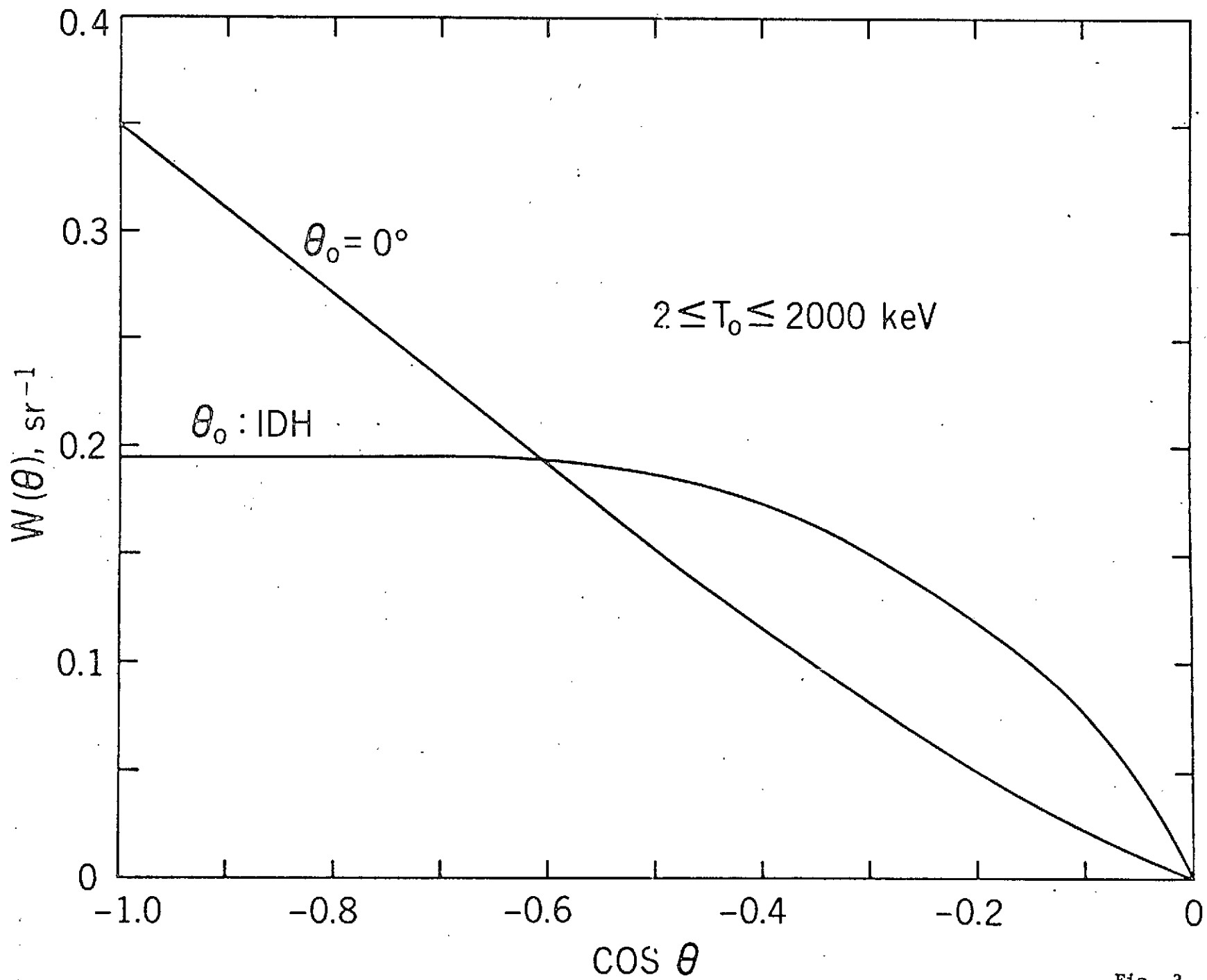
Fig. 3
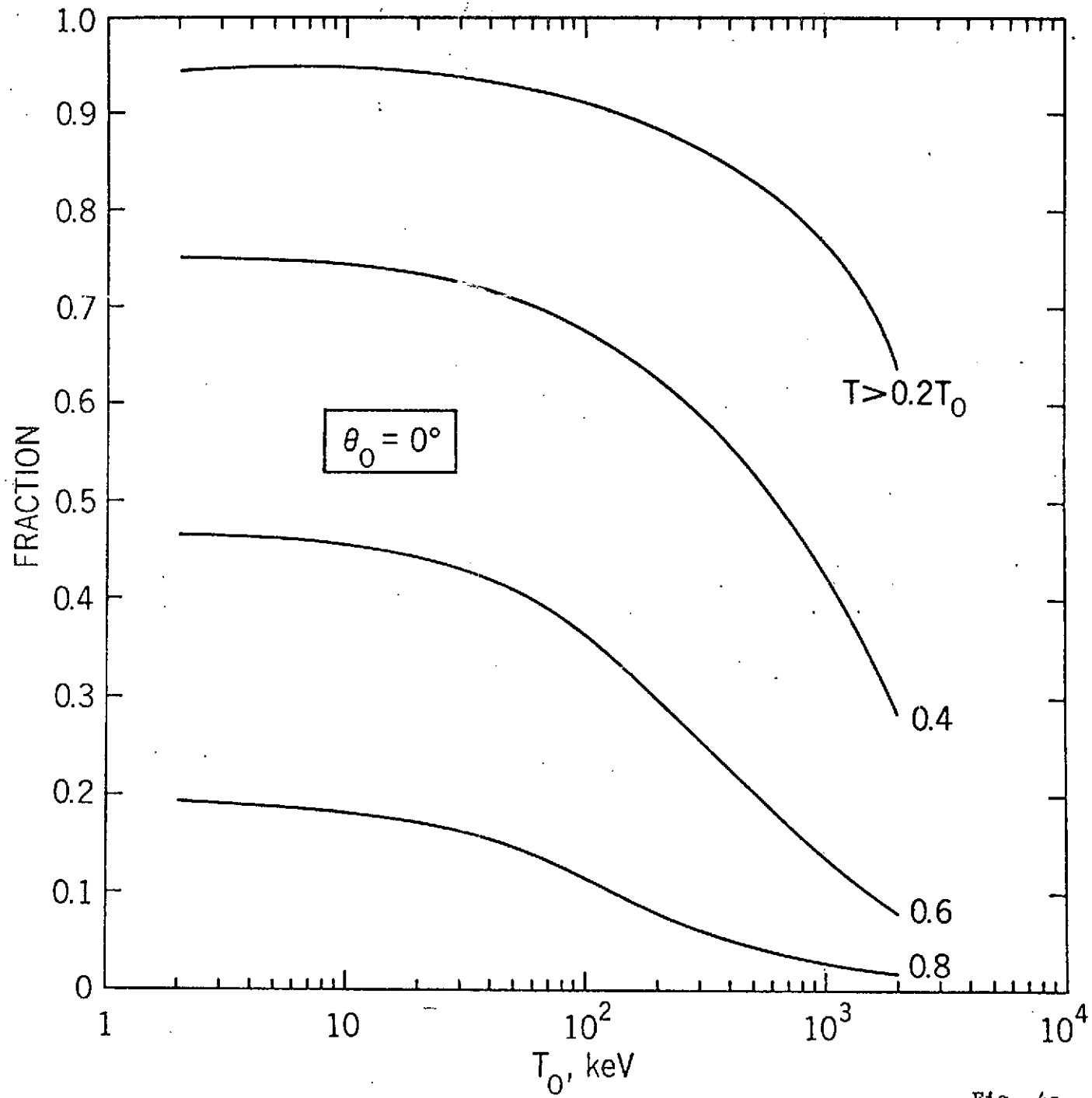
Fig. 4a

Fig. 4b

Fig. 5a

Fig. 5b

Fig. 5c

ENERGY DEPOSITION BY ELECTRONS

$$S(T_0) = \frac{1}{\alpha} e^{-T_0/\alpha}$$

θ_0:IDH

Fig. 6

ENERGY DEPOSITION BY BREMSSTRAHLUNG

$$S(T_0) = \frac{1}{\alpha} e^{-T_0/\alpha}$$
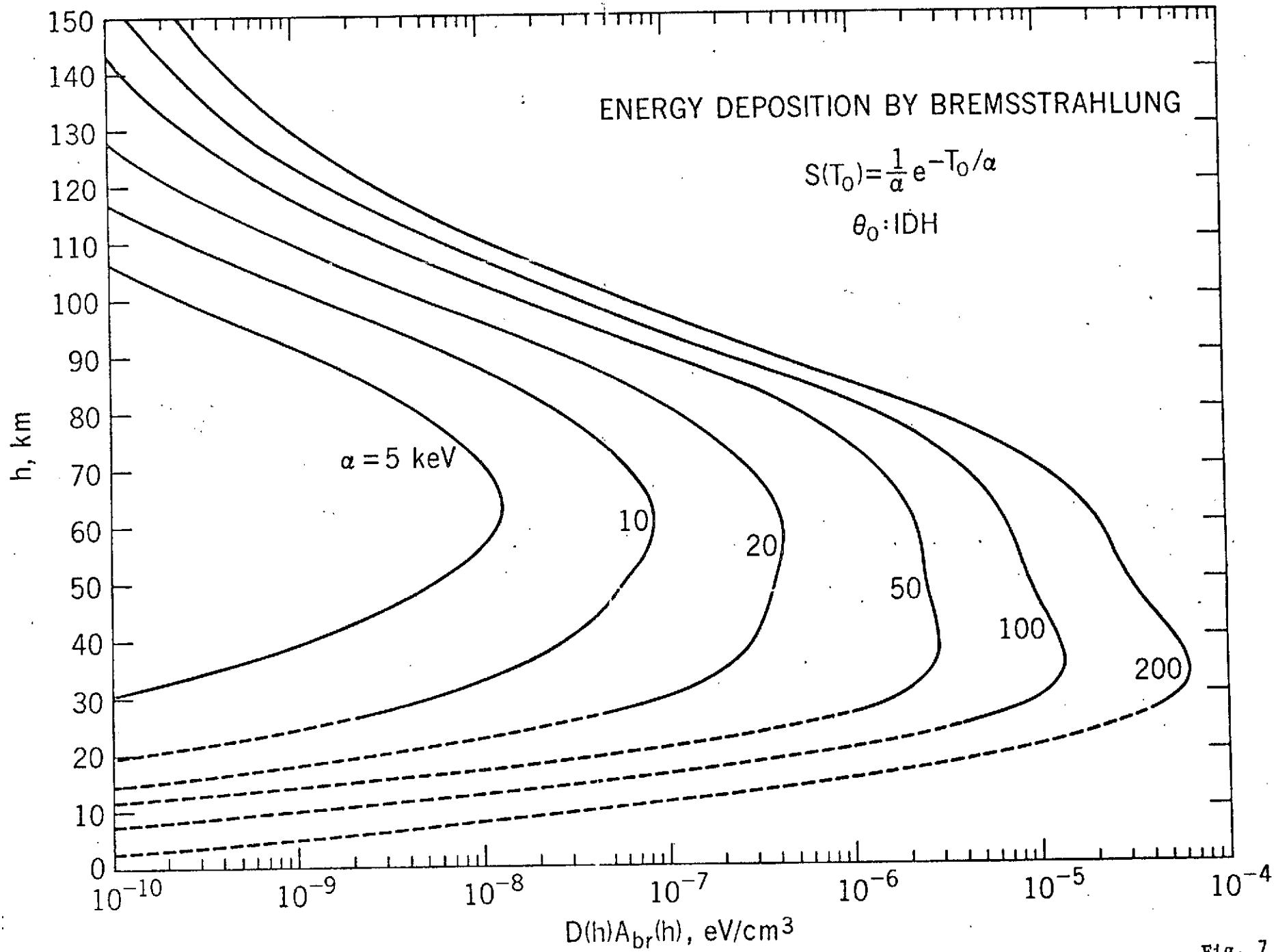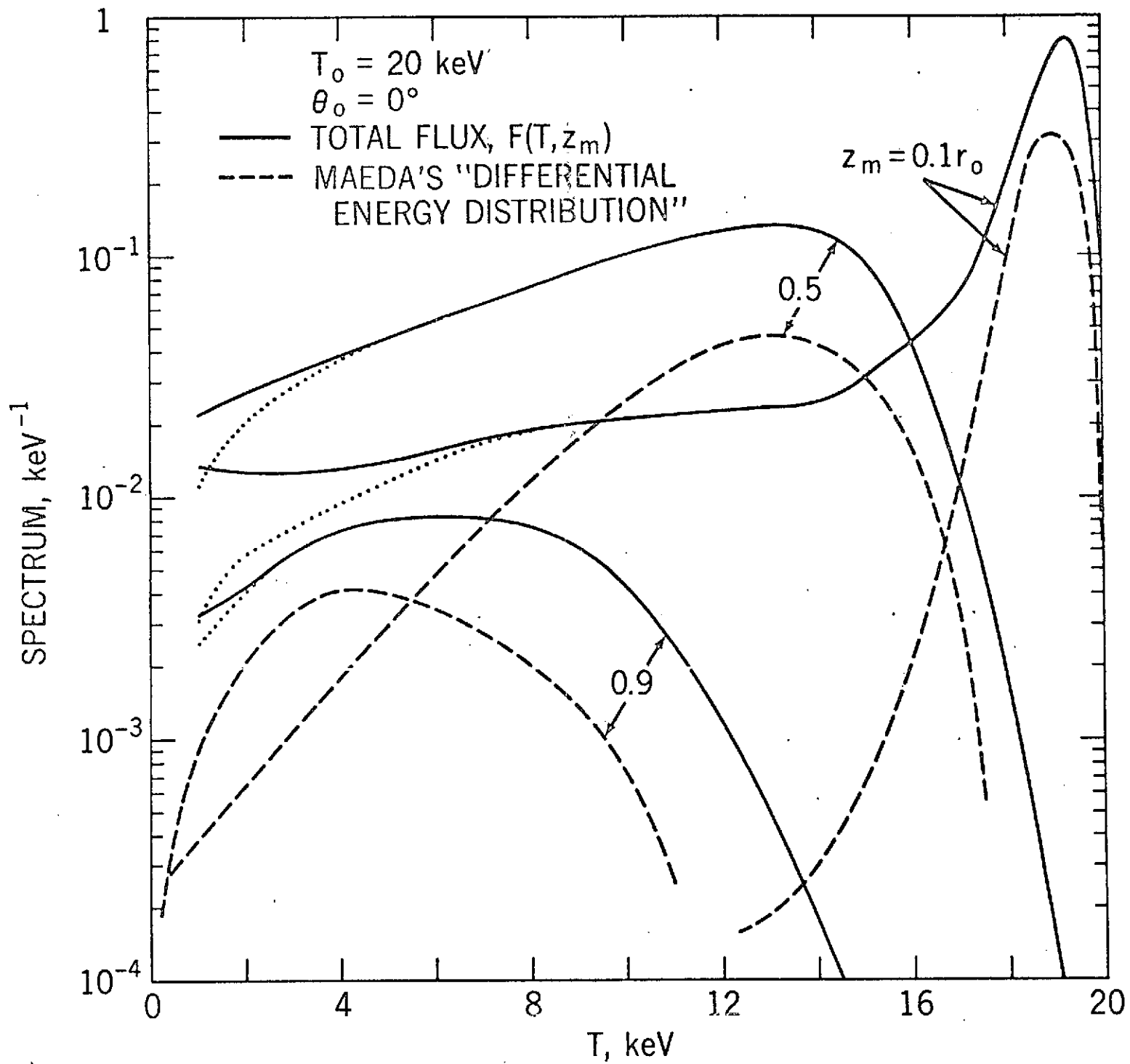
θ_0:IDH

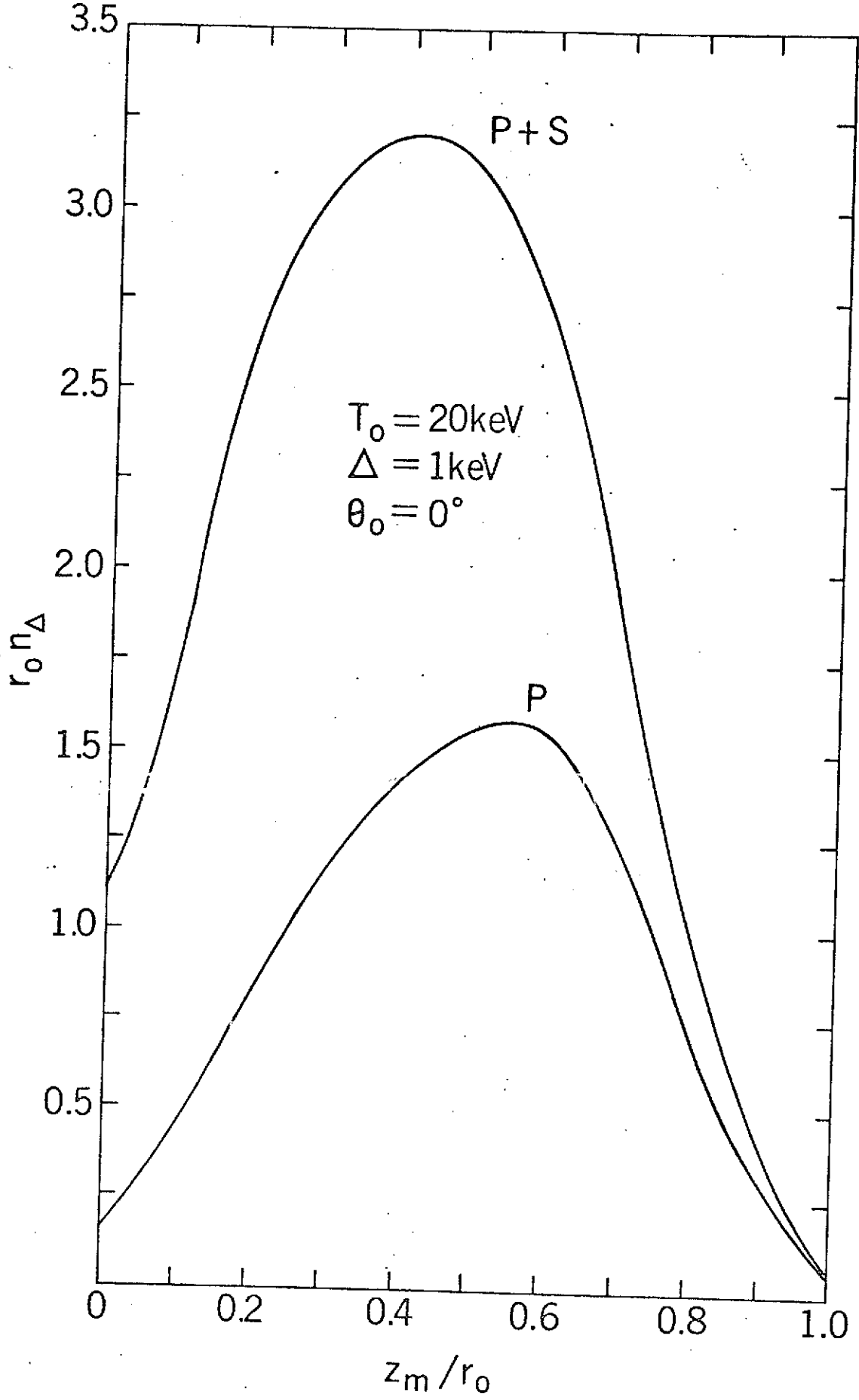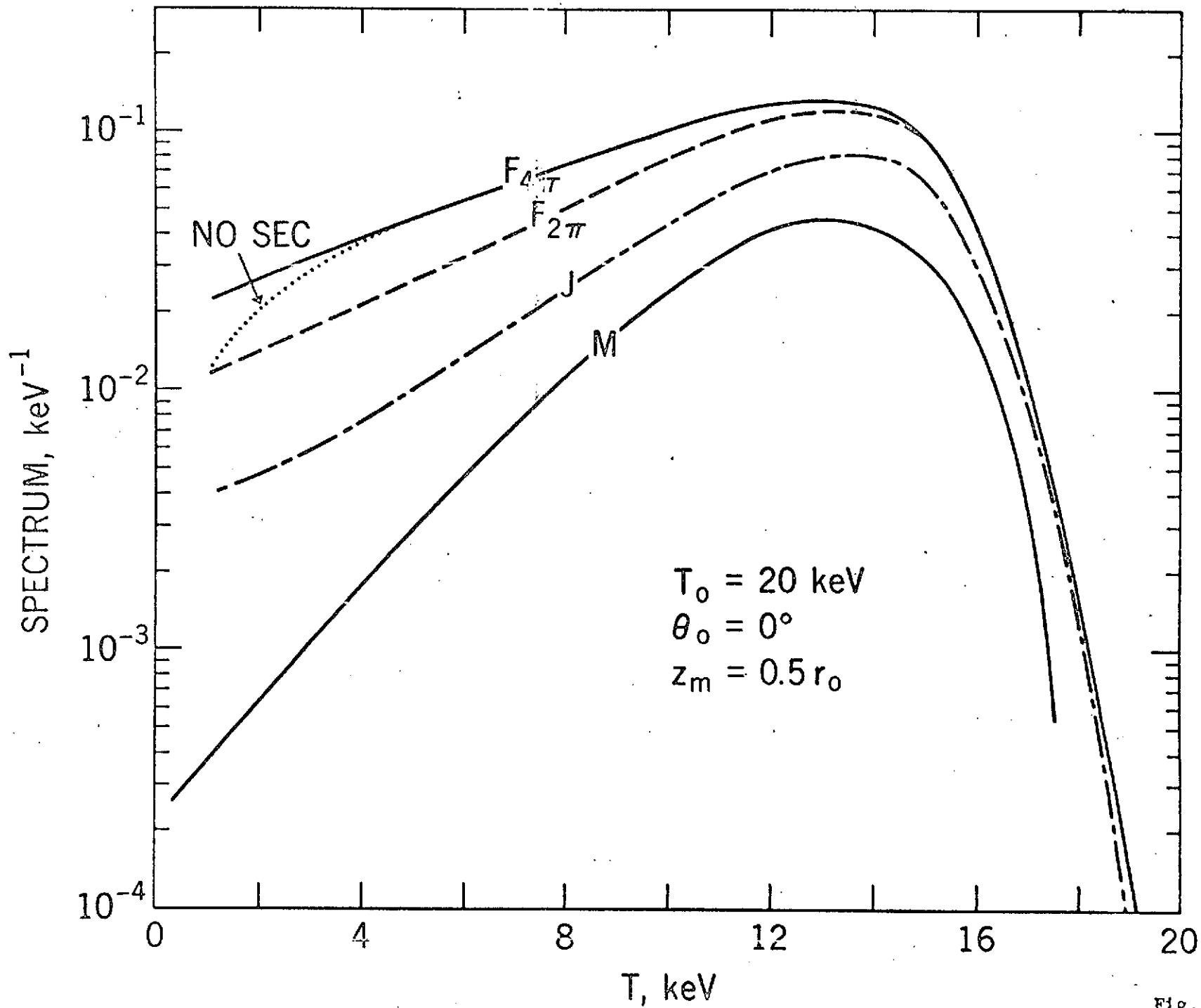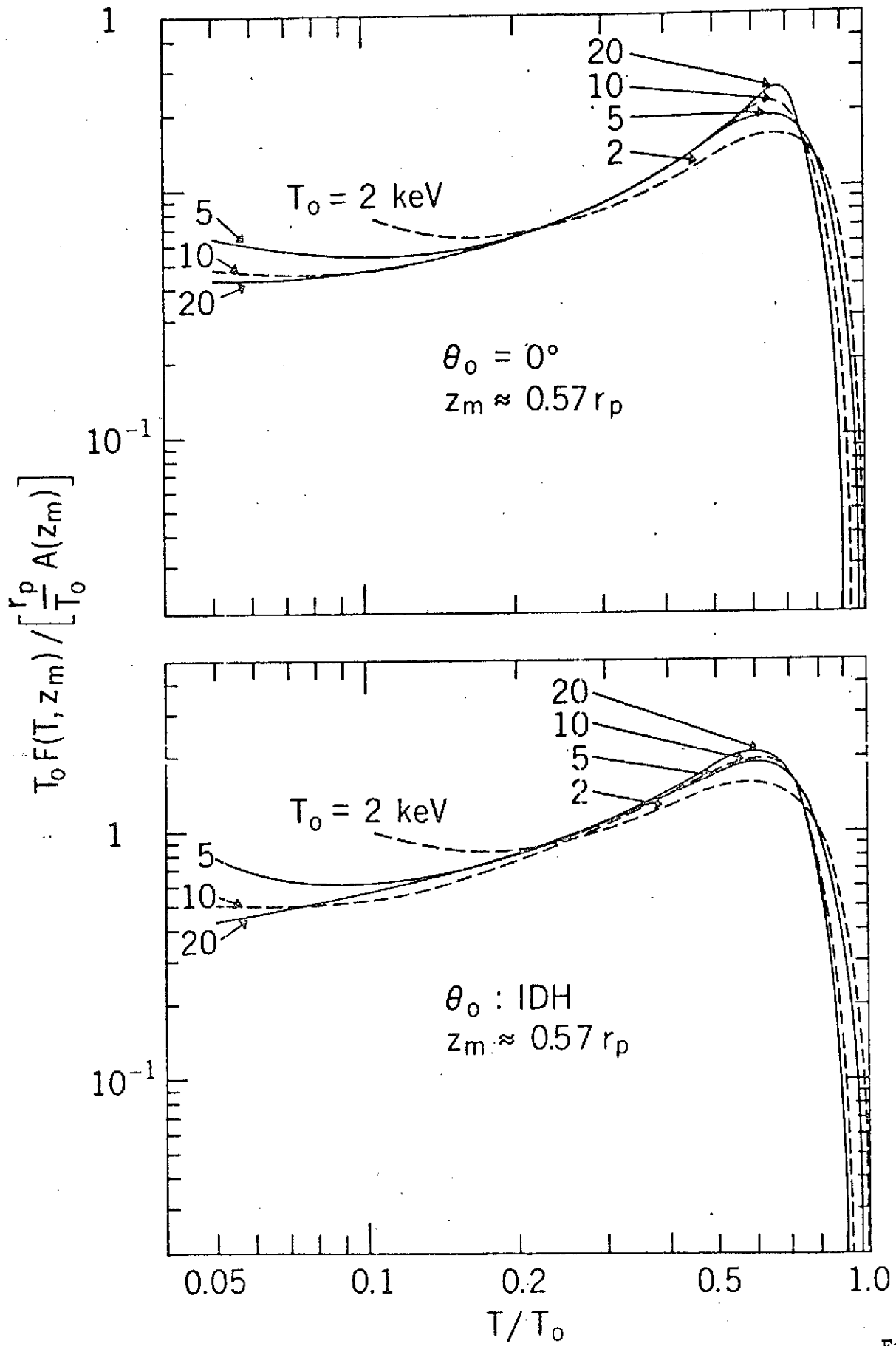$\alpha = 5$ keV

10

20

50

100

200

h, km

$D(h)A_{br}(h)$, eV/cm³
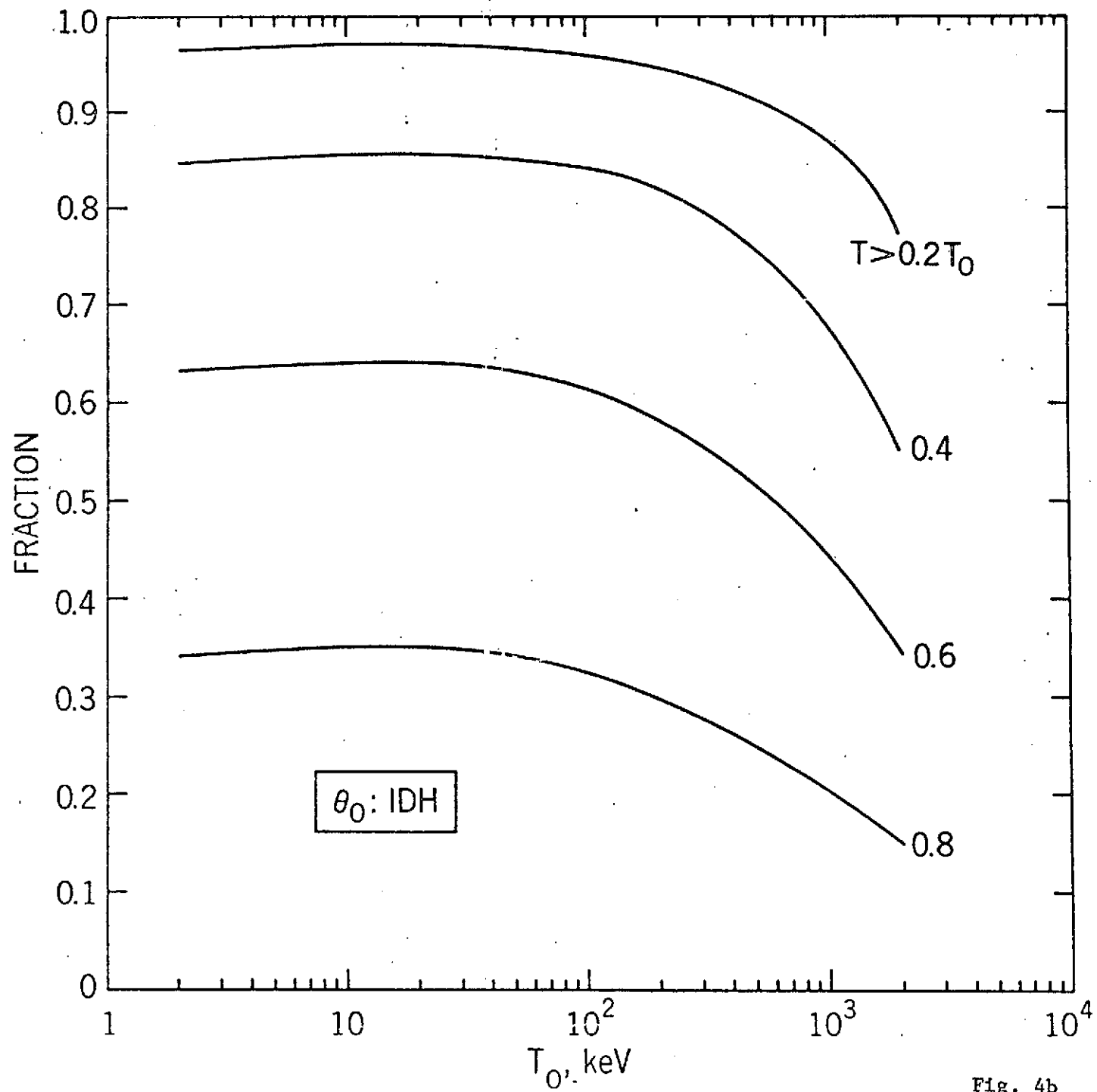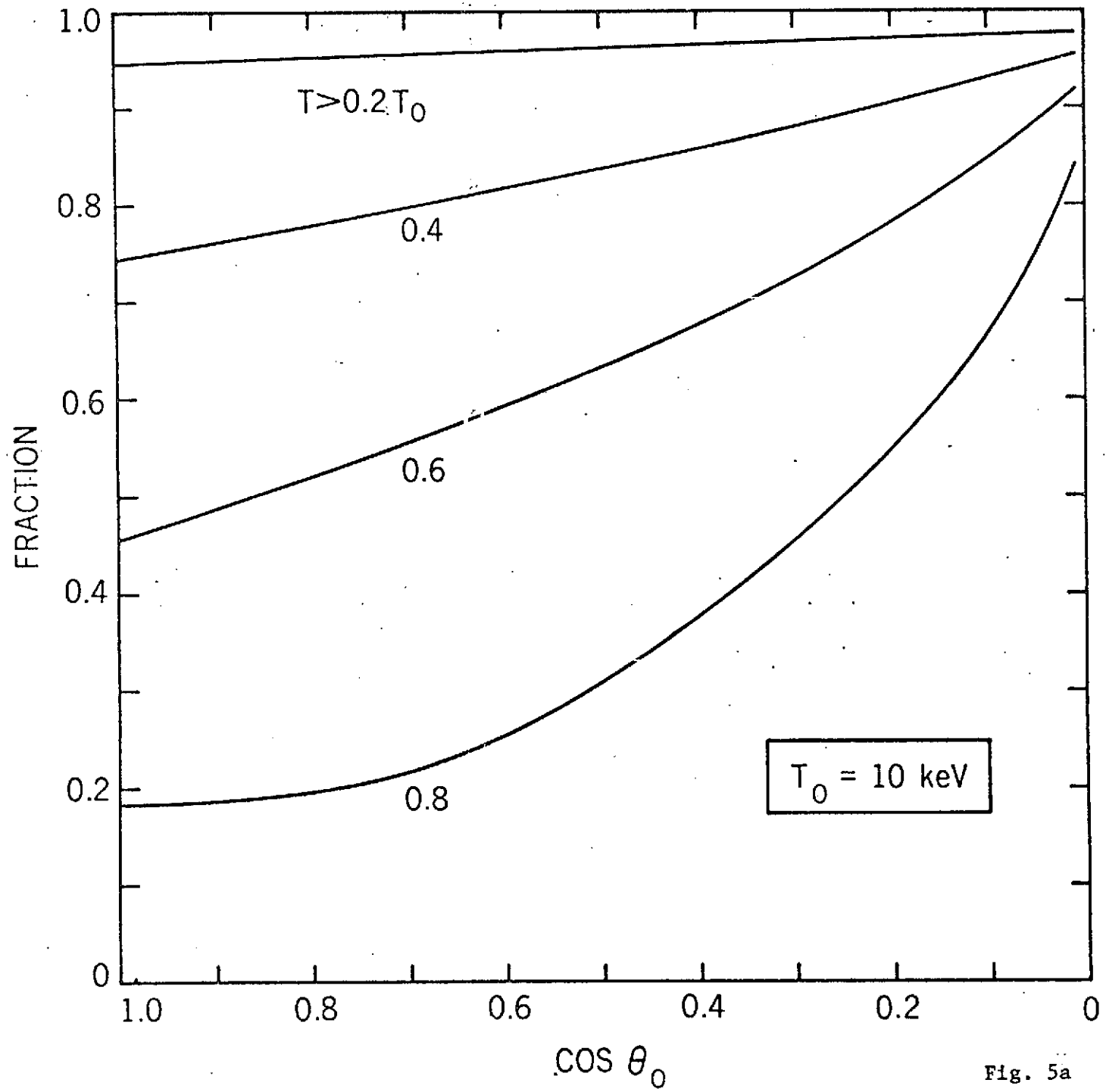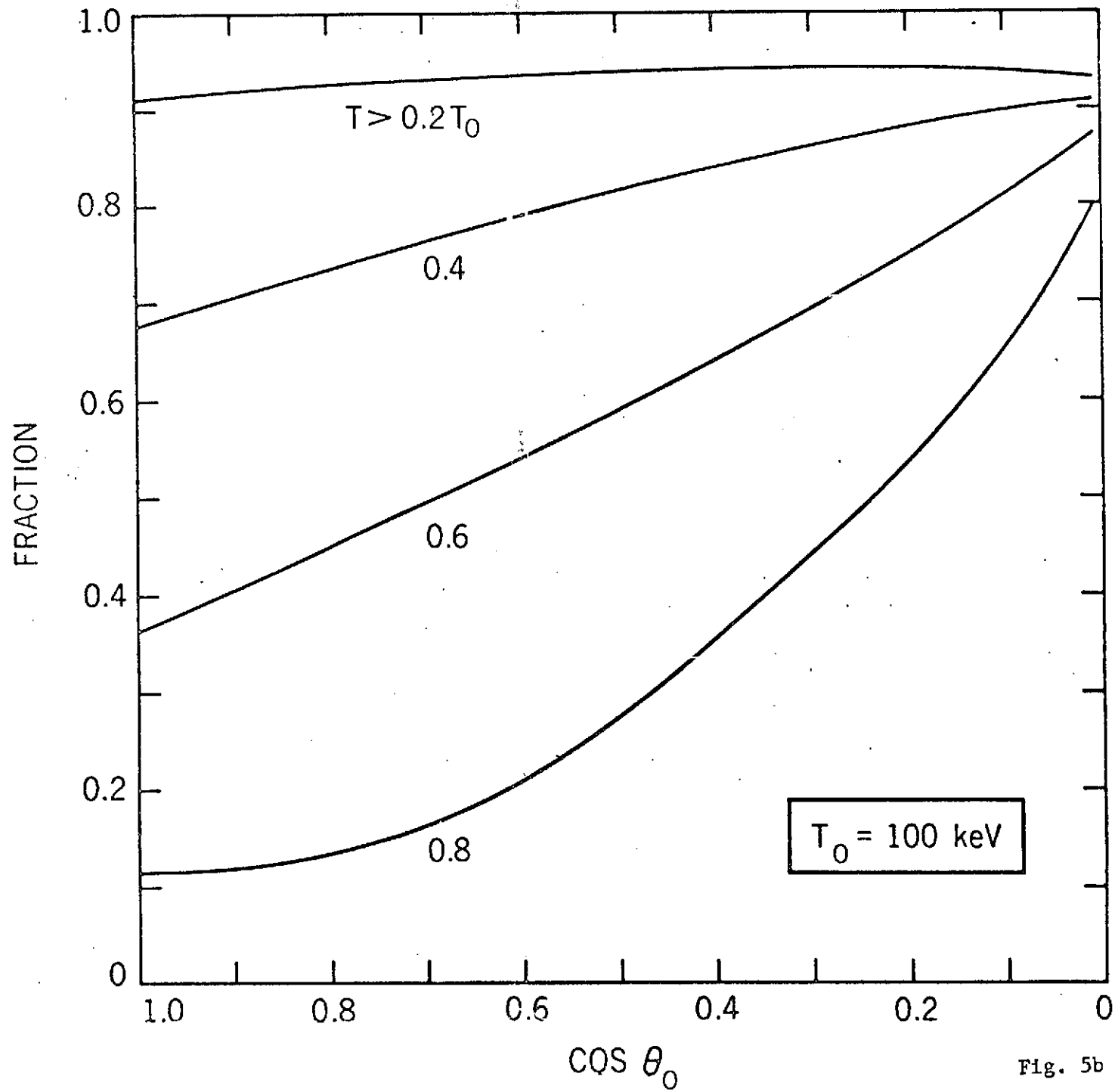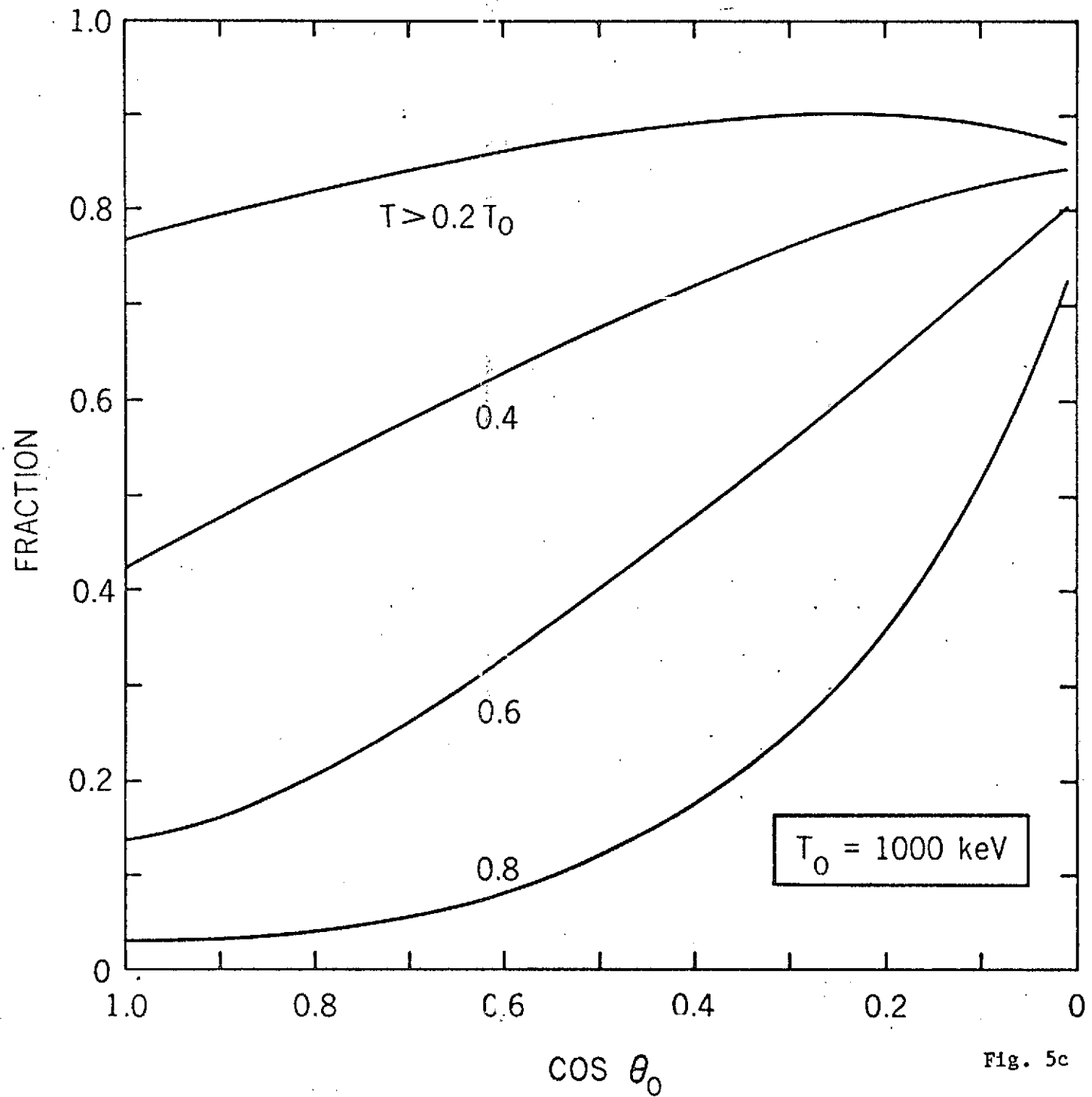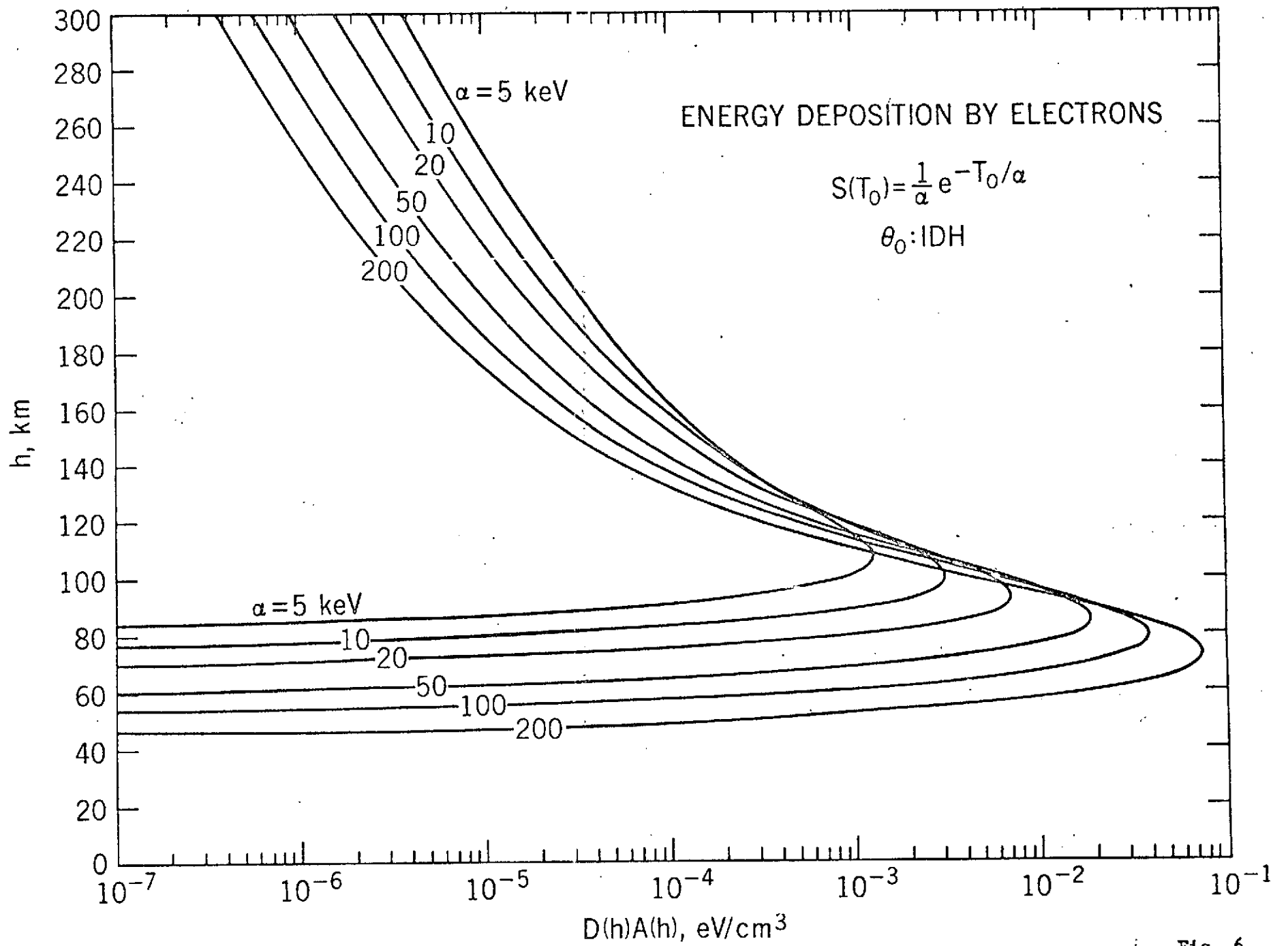
Fig. 7

Fig. 8

Fig. 9

Fig. 10

Fig. 11

Fig. 12

Fig. 13

Fig. 14